Supplementary Materials

Customization of functional MOFs by a modular design strategy for target applications

Yaguang Peng[1,2], Qiang Tan[1], Hongliang Huang[1,*], Qinggong Zhu[2], Xinchen Kang[2,3,*], Chongli Zhong[1], Buxing Han[2,3,*]

[1]State Key Laboratory of Separation Membranes and Membrane Processes, School of Chemical Engineering and Technology, Tiangong University, Tianjin 300387, China.
[2]Beijing National Laboratory for Molecular Sciences, Key Laboratory of Colloid, Interface and Thermodynamics, CAS Research/Education Center for Excellence in Molecular Sciences, Institute of Chemistry, Chinese Academy of Sciences, Beijing 100190, China.
[3]School of Chemistry, University of Chinese Academy of Sciences, Beijing 100049, China.

***Correspondence to:** Prof./Dr. Hongliang Huang, State Key Laboratory of Separation Membranes and Membrane Processes, School of Chemical Engineering and Technology, Tiangong University, No. 399 BinShuiXi Road, Tianjin 300387, China. E-mail: huanghongliang@tiangong.edu.cn; Prof./Dr. Xinchen Kang, Beijing National Laboratory for Molecular Sciences, Key Laboratory of Colloid, Interface and Thermodynamics, CAS Research/Education Center for Excellence in Molecular Sciences, Institute of Chemistry, Chinese Academy of Sciences, No. 2 Zhongguancun North First Street, Beijing 100190, China. E-mail: kangxinchen@iccas.ac.cn; Prof./Dr. Buxing Han, Beijing National Laboratory for Molecular Sciences, Key Laboratory of Colloid, Interface and Thermodynamics, CAS Research/Education Center for

Excellence in Molecular Sciences, Institute of Chemistry, Chinese Academy of Sciences, No. 2 Zhongguancun North First Street, Beijing 100190, China. E-mail: hanbx@iccas.ac.cn

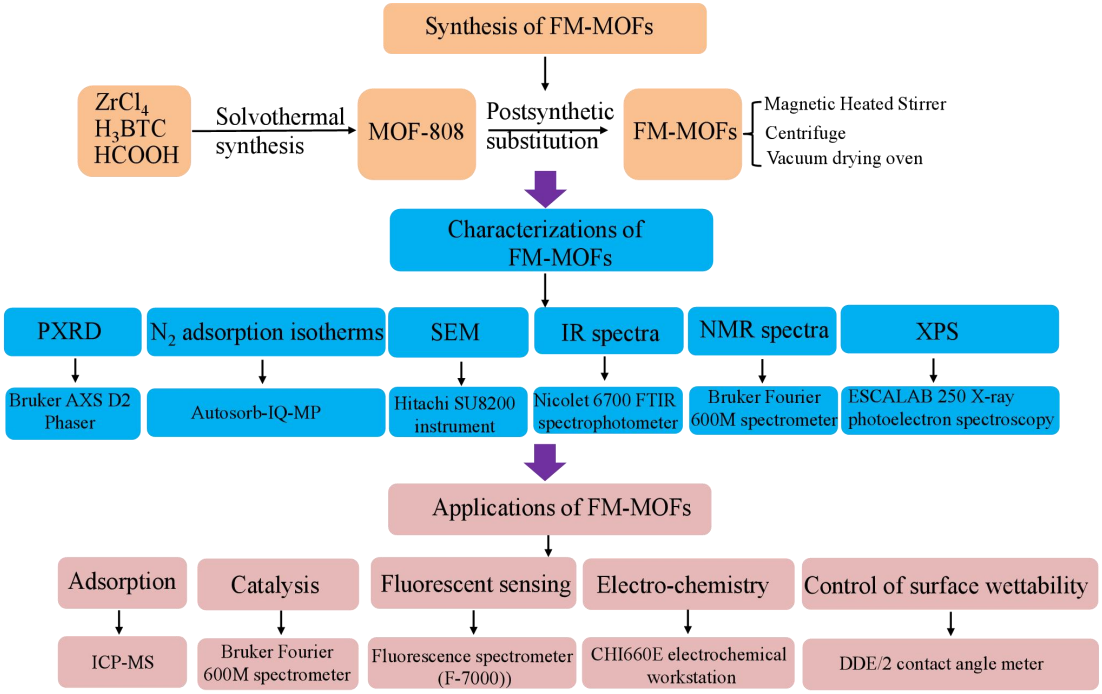

Supplementary Figure 1. The experimental devices used for material synthesis, characterization, and application.

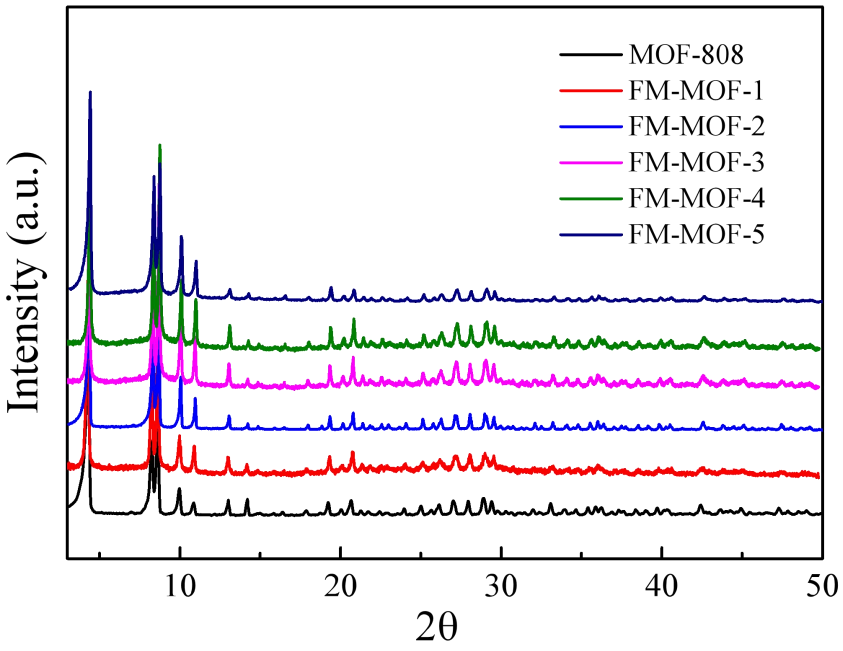

Supplementary Figure 2. PXRD patterns of MOF-808 and its derived FM-MOFs.

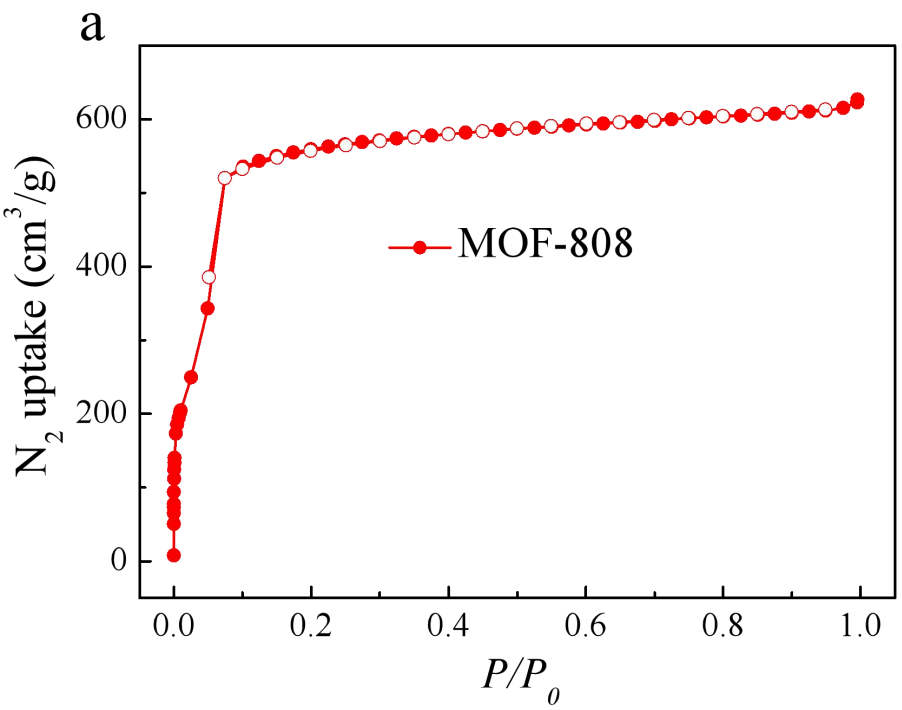

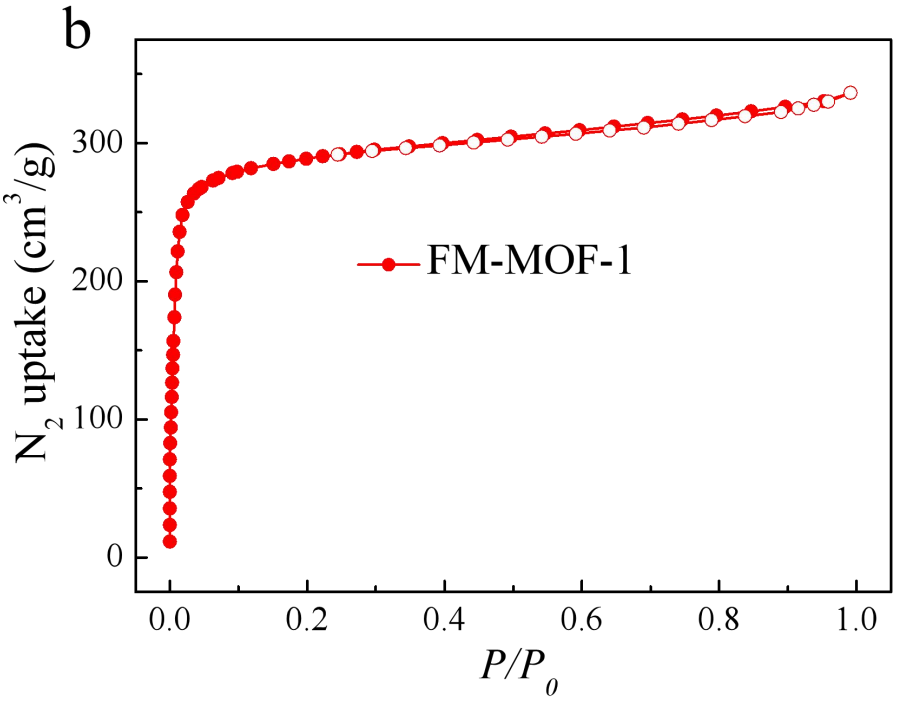
b
300
200
100
0
N_2 uptake (cm^3/g)
FM-MOF-1
0.0
0.2
0.4
0.6
0.8
1.0
P/P_0

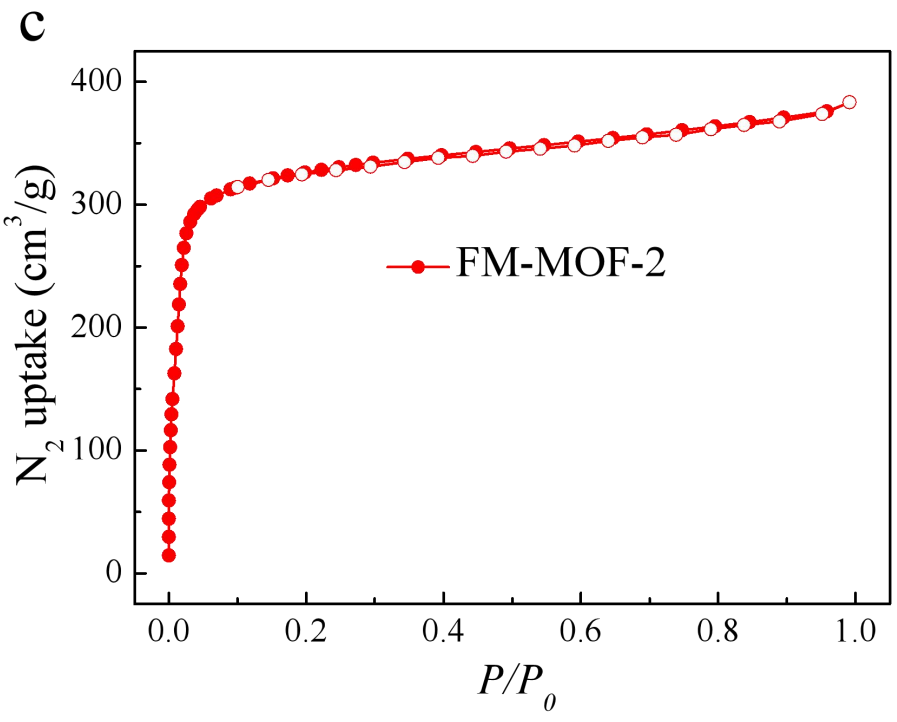
c
400
300
200
100
0
N_2 uptake (cm^3/g)
FM-MOF-2
0.0
0.2
0.4
0.6
0.8
1.0
P/P_0

d

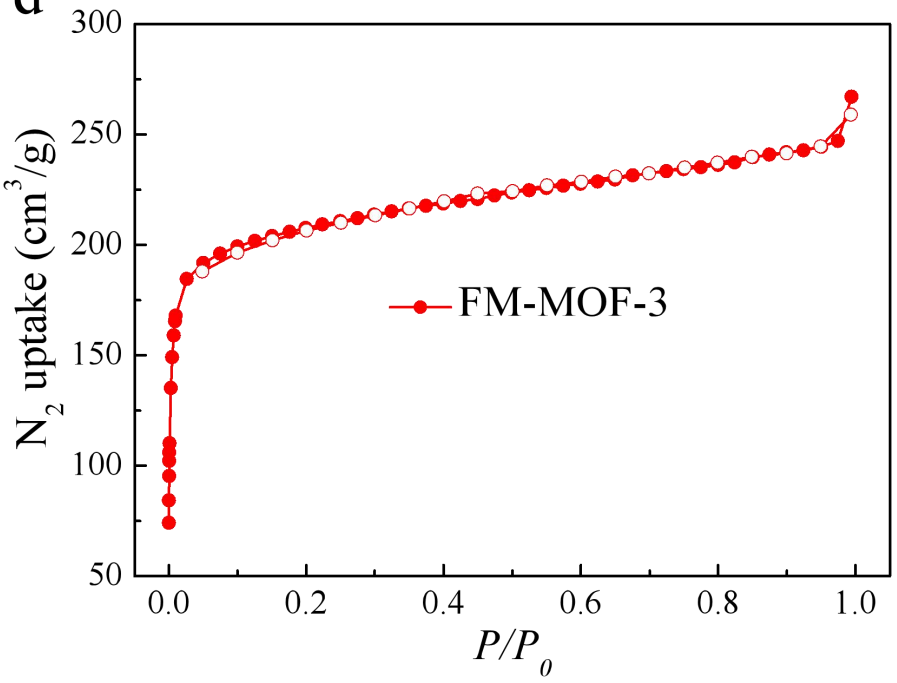
300
250
200
150
100
50
N2 uptake (cm3/g)
FM-MOF-3
0.0
0.2
0.4
0.6
0.8
1.0
P/P0

e

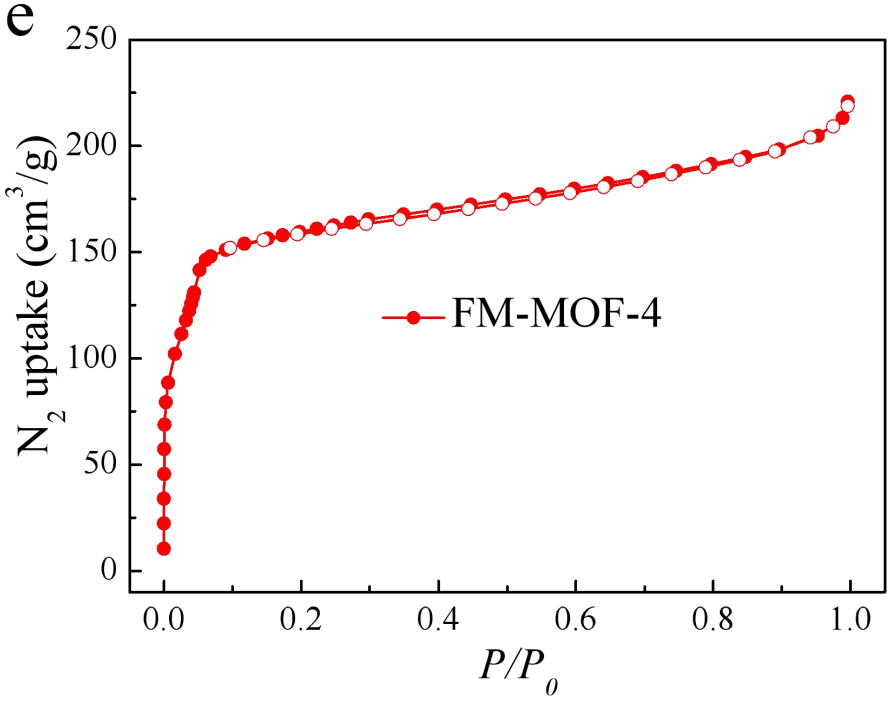
250
200
150
100
50
0
N2 uptake (cm3/g)
FM-MOF-4
0.0
0.2
0.4
0.6
0.8
1.0
P/P0

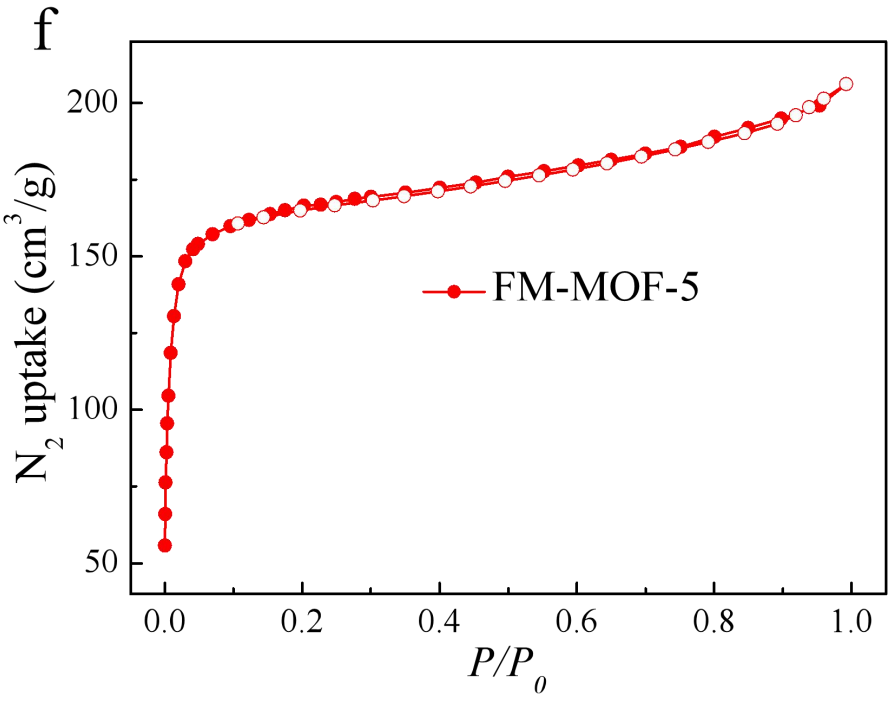

Supplementary Figure 3. N_2 adsorption-desorption isotherms of MOF-808 and its derived FM-MOFs. The BET surface areas were calculated to be 2424 $m^2 g^{-1}$ for (a), 1150 $m^2 g^{-1}$ for (b), 1482 $m^2 g^{-1}$ for (c), 813 $m^2 g^{-1}$ for (d), 587 $m^2 g^{-1}$ for (e) and 670 $m^2 g^{-1}$ for (f).

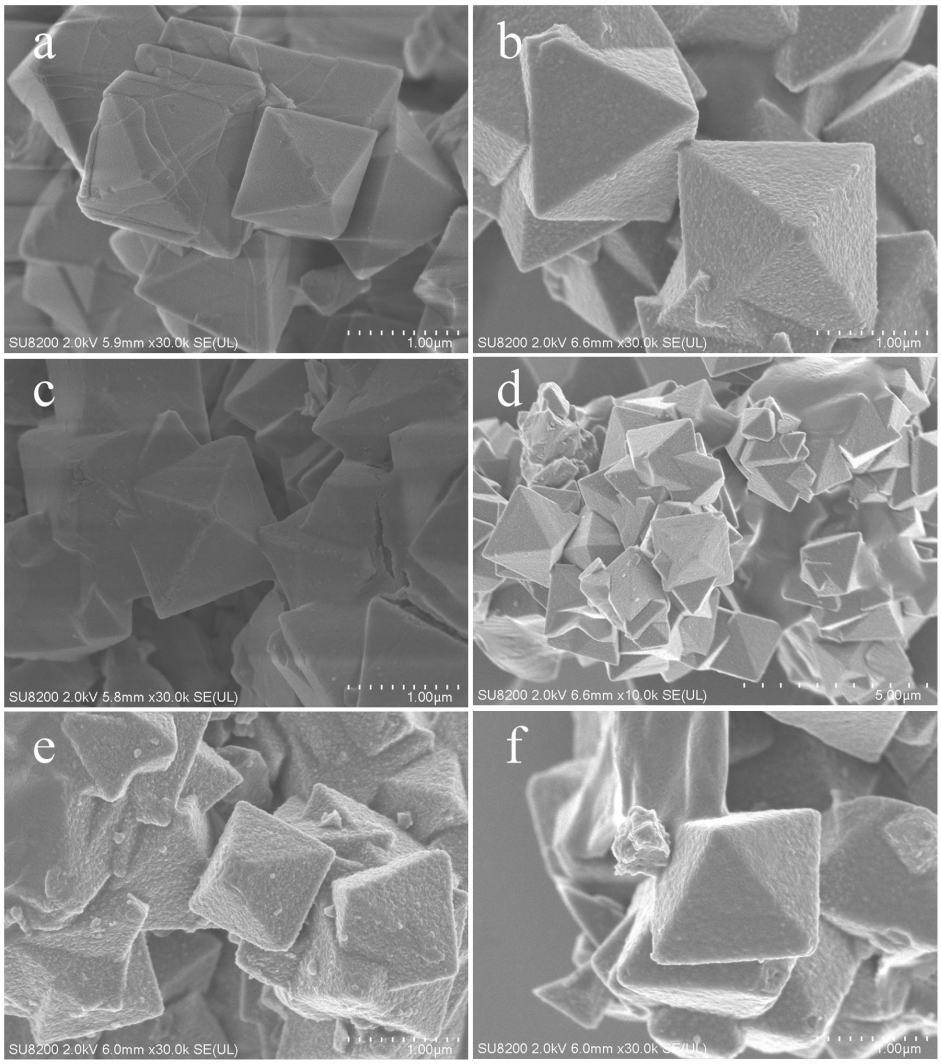

Supplementary Figure 4. SEM images of (a) MOF-808, (b) FM-MOF-1, (c) FM-MOF-2, (d) FM-MOF-3, (e) FM-MOF-4 and (f) FM-MOF-5.

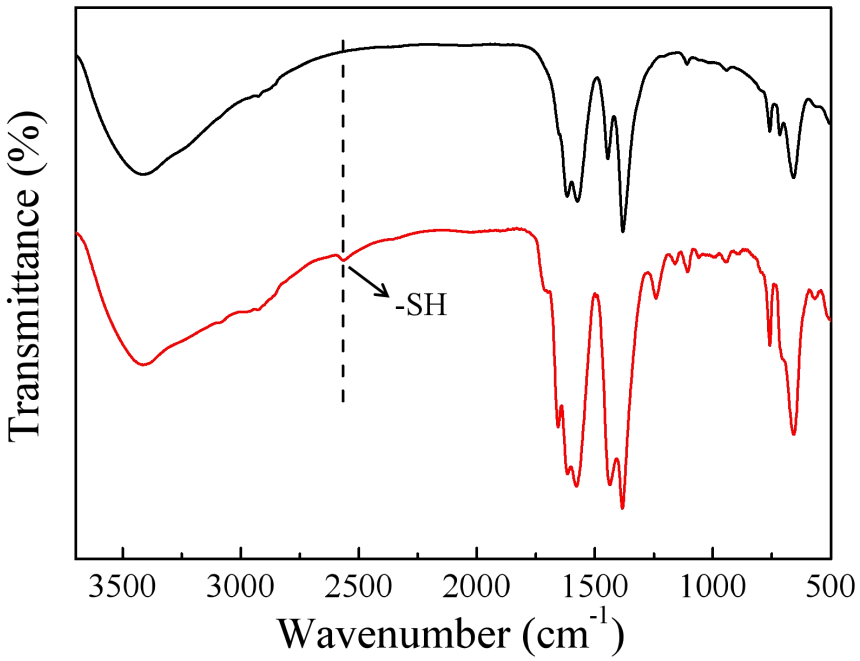

Supplementary Figure 5. FT-IR spectra of MOF-808 (black) and FM-MOF-1 (red).

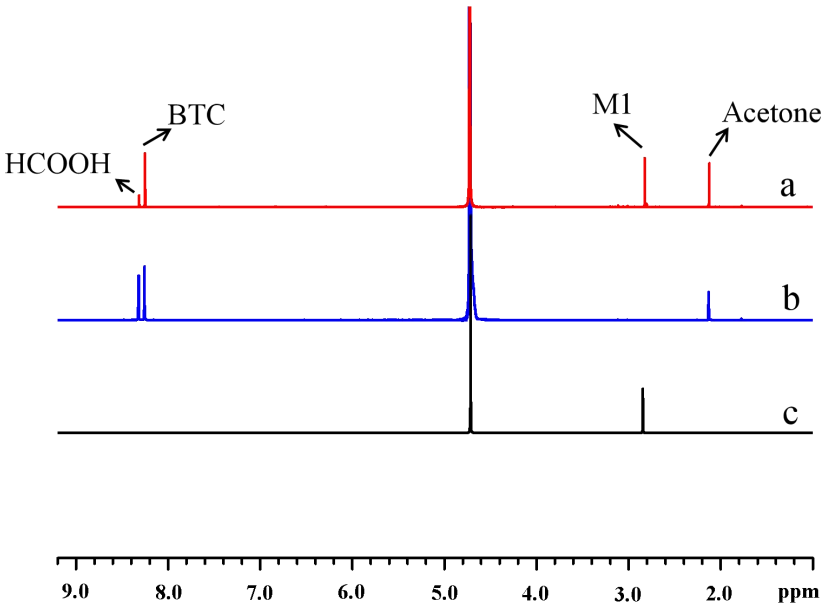

Supplementary Figure 6. ^{1}H NMR spectra of (a) alkaline-digested FM-MOF-1, (b) MOF-808, and (c) M1 (thioglycolic acid) in KOH/D_2O solution.

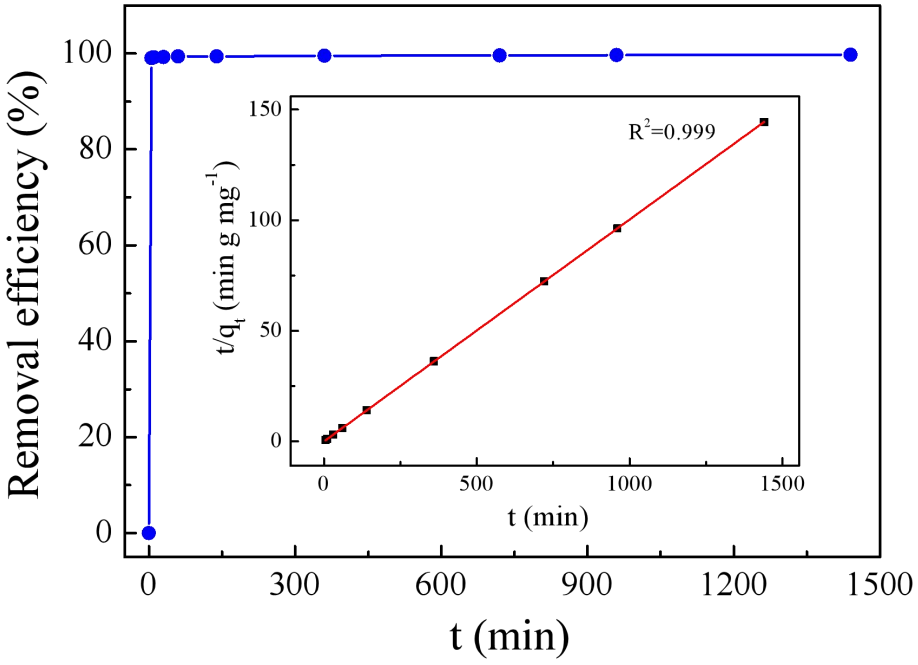

Supplementary Figure 7. Kinetics investigation of FM-MOF-1 for Hg^{2+} adsorption. Inset shows the pseudo-second-order kinetic plot for the adsorption.

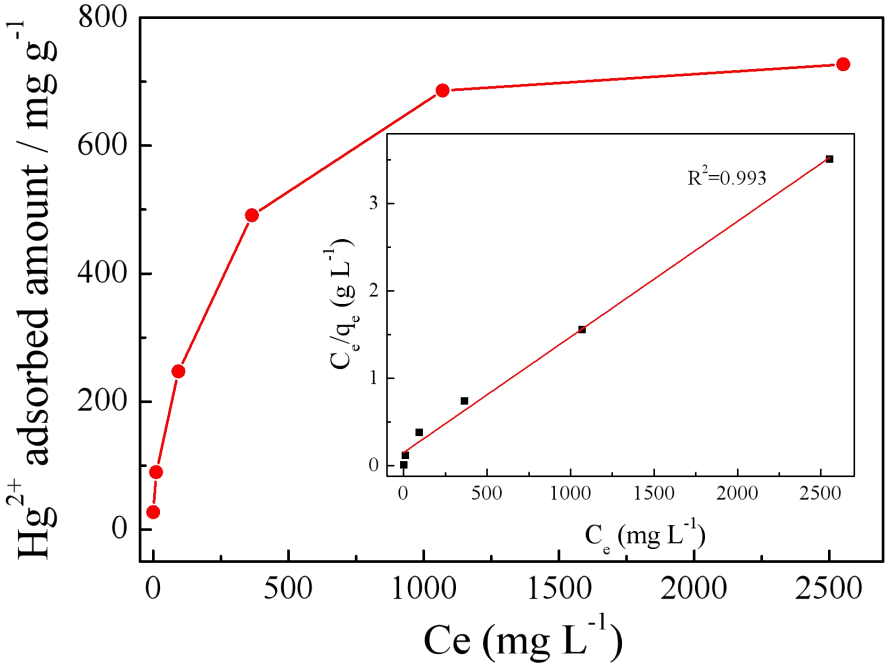

Supplementary Figure 8. Hg^{2+} adsorption isotherm of FM-MOF-1. Inset shows the linear regression by fitting the experimental data with the Langmuir model.

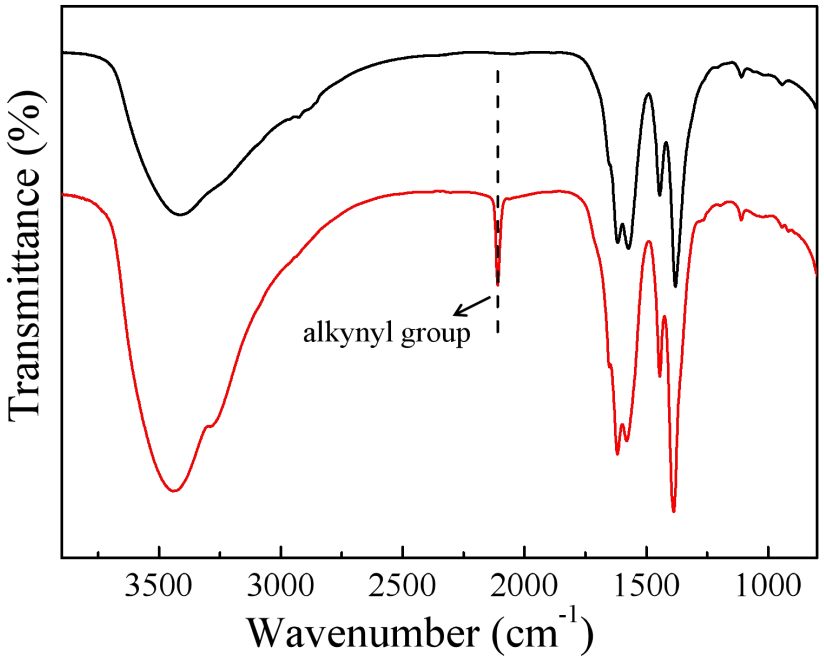

Supplementary Figure 9. FT-IR spectra of MOF-808 (black) and FM-MOF-2 (red). FM-MOF-3 exhibits a new peak at 2110 cm^{-1}, which can be attributed to the stretching frequency of the alkynyl group in M2 (propiolic acid).

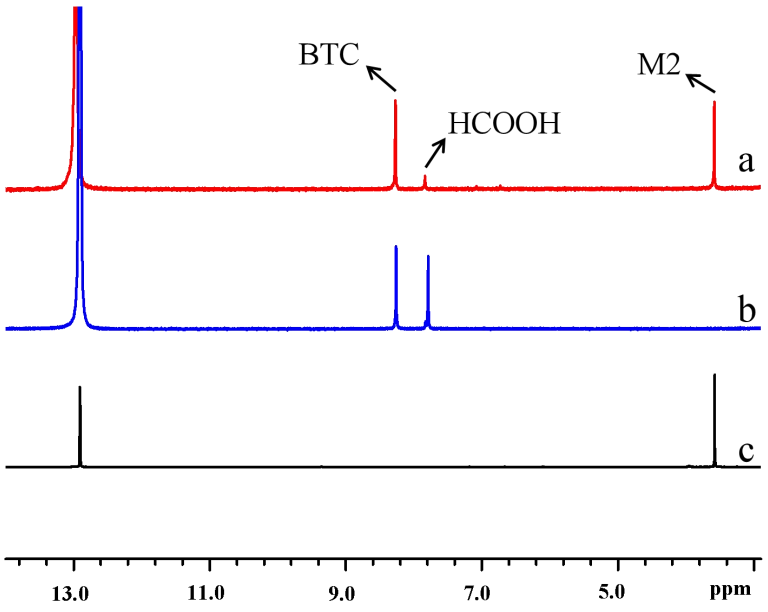

Supplementary Figure 10. ^{1}H NMR spectra of (a) acid-digested FM-MOF-2, (b) MOF-808, and (c) M2 (propiolic acid) in DMSO/D_2SO_4 solution. It is obvious that the signal of the formate group in FM-MOF-2 almost disappears and a new peak corresponding to the hydrogen of M2 emerges, indicating the formate ligands on Zr_6 clusters in MOF-808 have been successfully substituted by M2.

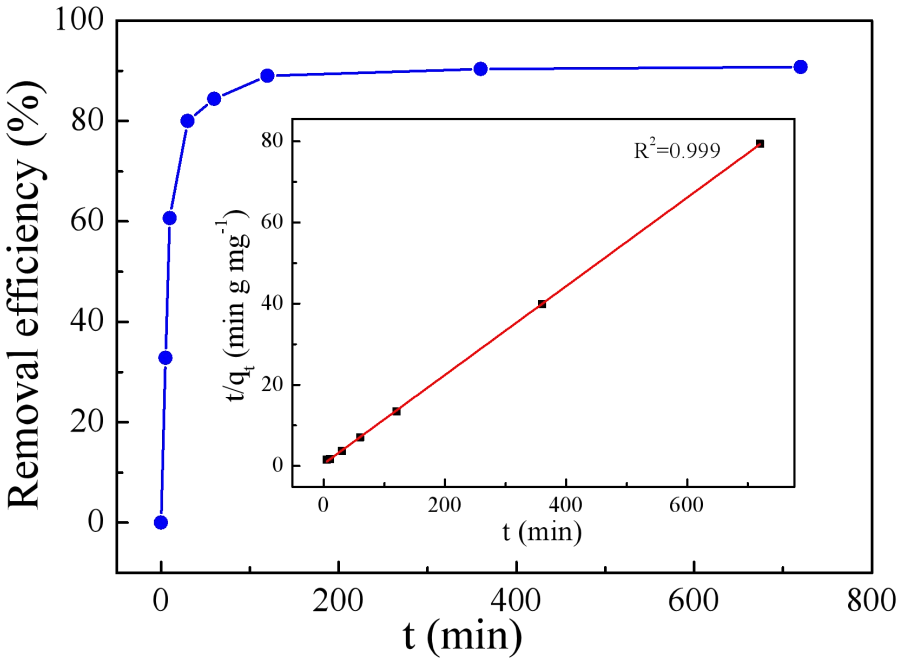

Supplementary Figure 11. Kinetics investigation of FM-MOF-2 for Ag^{+} adsorption. Inset shows the pseudo-second-order kinetic plot for the adsorption.

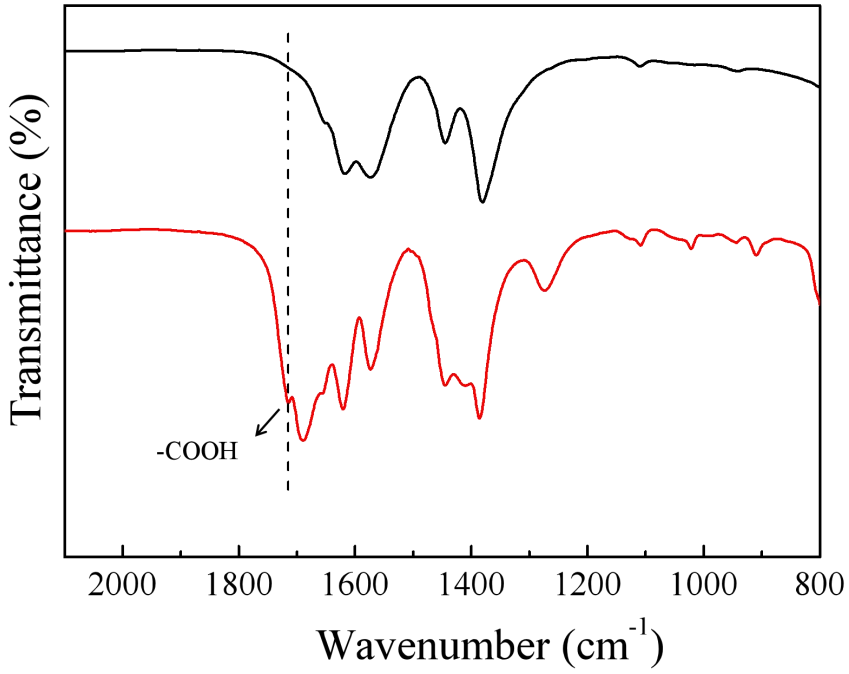

Supplementary Figure 12. FT-IR spectra of FM-MOF-3 (red) and MOF-808 (black). FM-MOF-3 exhibits a new peak at 1715 cm^{-1}, which can be attributed to the stretching frequency of the free carboxylic group in M3 (oxalic acid).

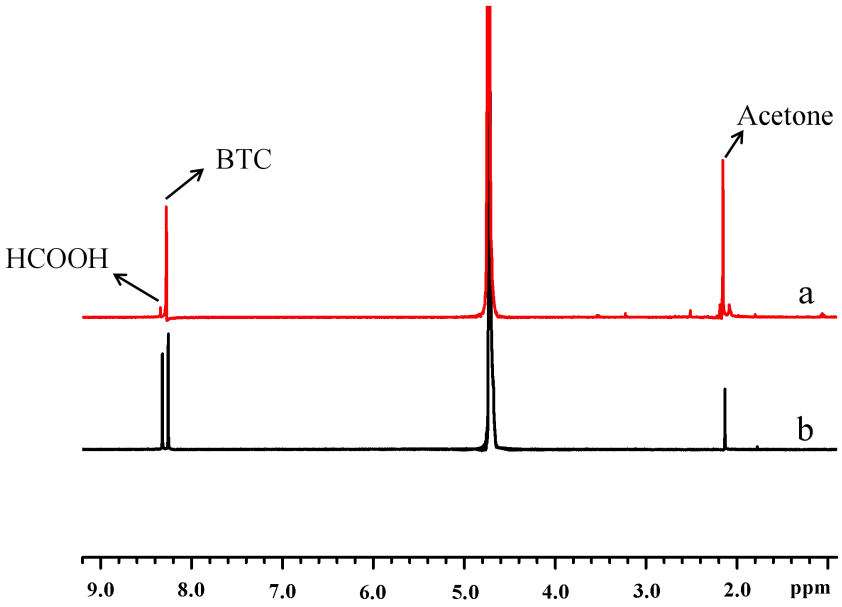

Supplementary Figure 13. ^{1}H NMR spectra of (a) alkaline-digested FM-MOF-3 and (b) MOF-808 in KOH/D_2O solution. It is obvious that the peak at 8.34 ppm for the

hydrogen of the formate group in FM-MOF-3 almost disappears, suggesting the formate ligands on Zr_6 clusters in MOF-808 have been successfully substituted by M3 (oxalic acid).

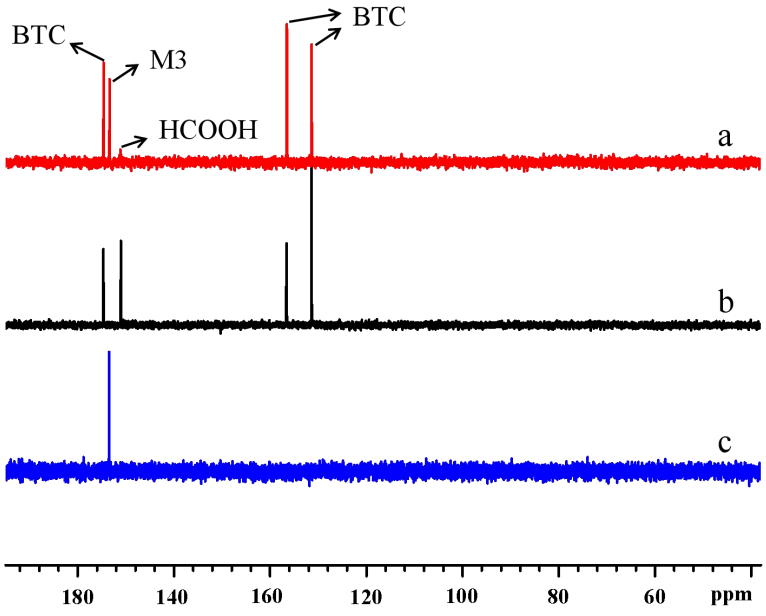

Supplementary Figure 14. ^{13}C NMR spectra of (a) alkaline-digested FM-MOF-3, (b) alkaline-digested MOF-808, and (c) M3 (oxalic acid) in KOH/D_2O solution. It is obvious that the peak at 171.1 ppm for the carbon of the formate group in FM-MOF-3 reduces significantly and one additional chemical shift at 173.4 ppm corresponding to the carbon signal of oxalic acid emerges, indicating most of the formate ligands on Zr_6 clusters are substituted by M3.

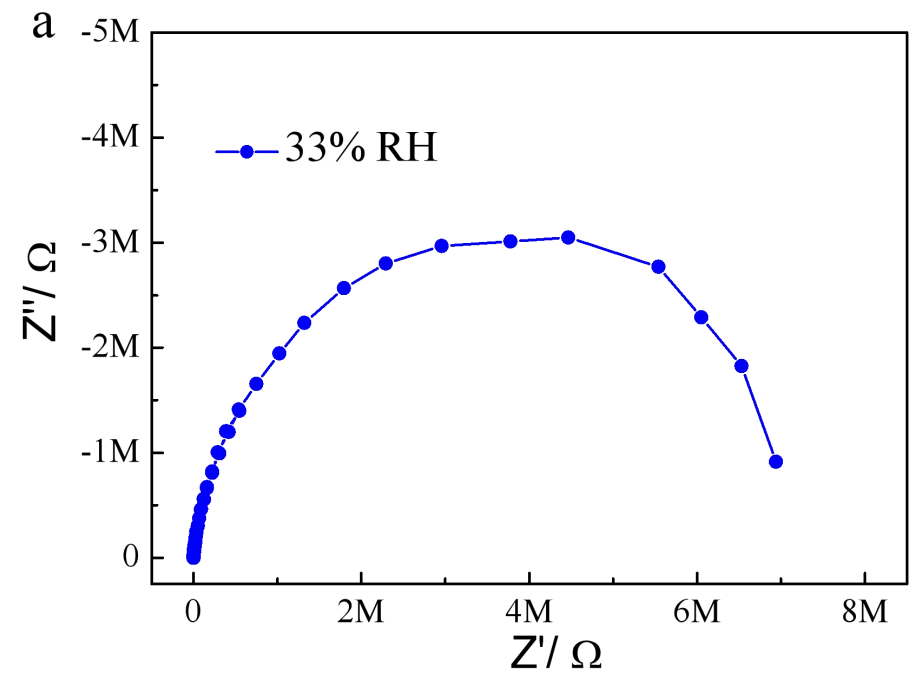
a
-5M
-4M
-3M
-2M
-1M
0
Z''/ Ω
33% RH
0
2M
4M
6M
8M
Z'/ Ω

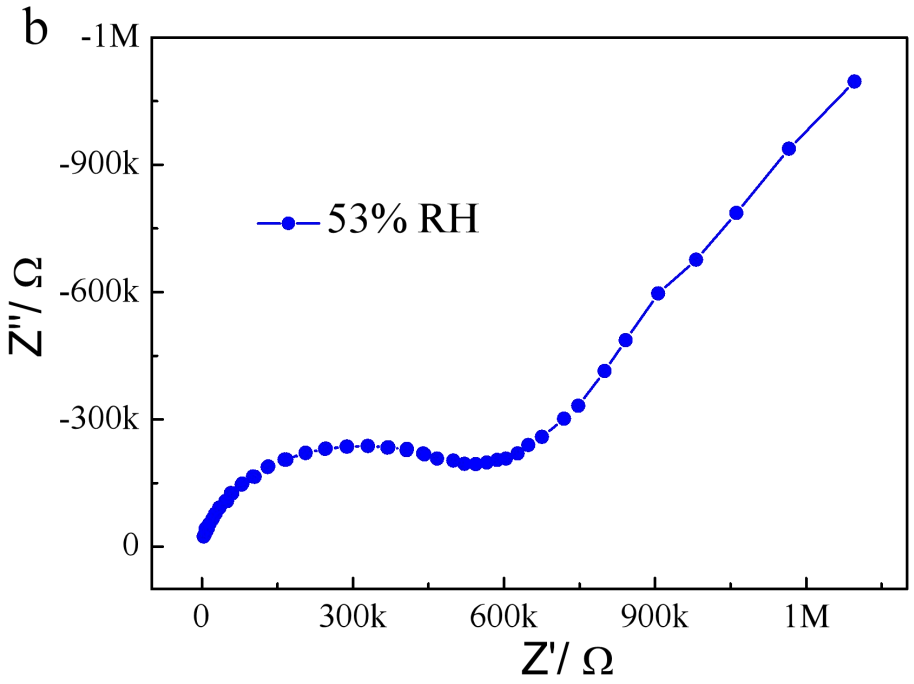
b
-1M
-900k
-600k
-300k
0
Z''/ Ω
53% RH
0
300k
600k
900k
1M
Z'/ Ω

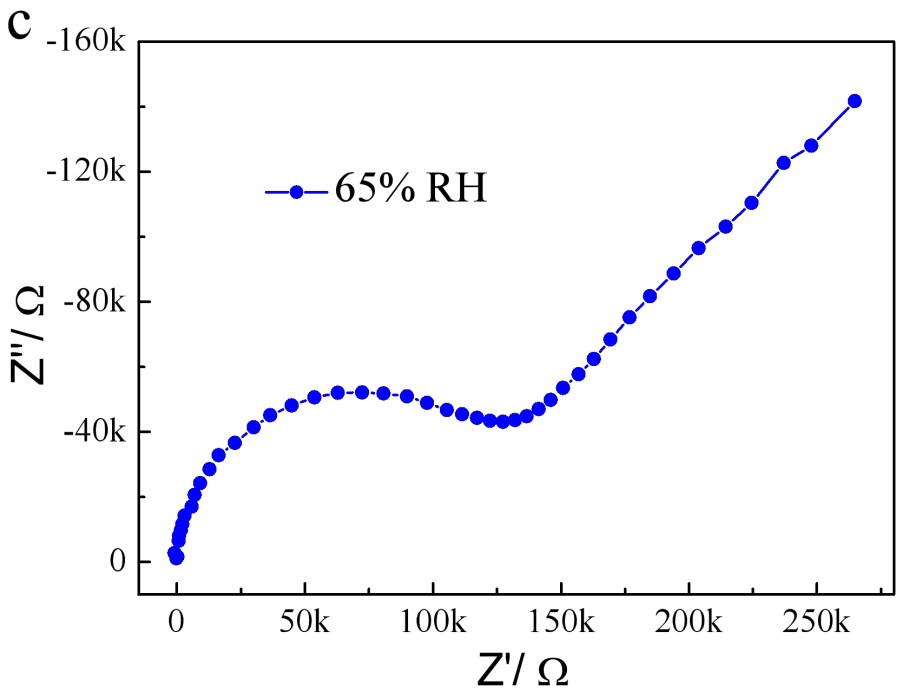
c
-160k
-120k
-80k
-40k
0
Z''/ Ω
65% RH
0
50k
100k
150k
200k
250k
Z'/ Ω

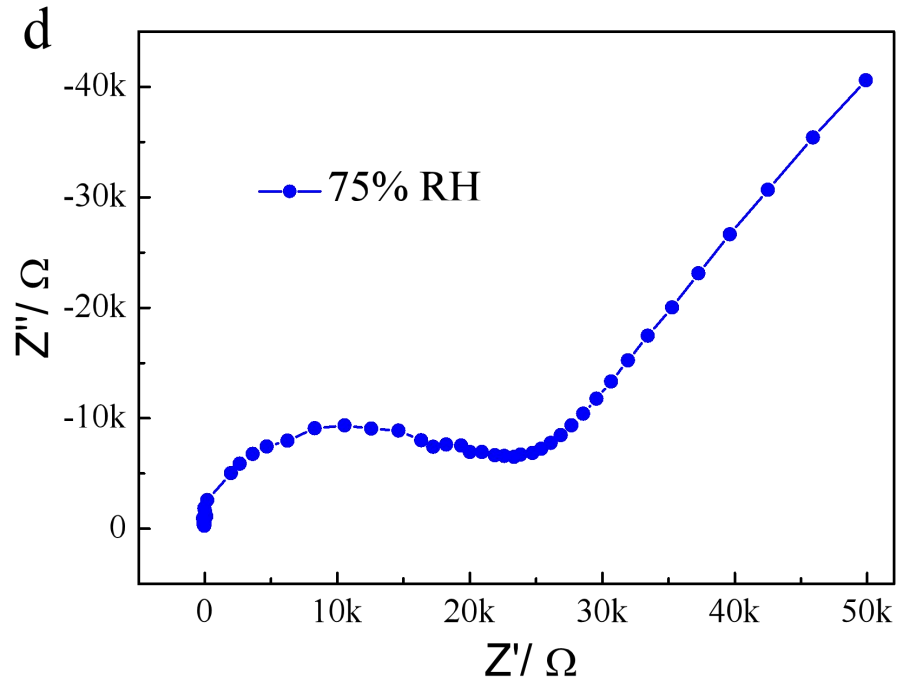
d
-40k
-30k
-20k
-10k
0
Z''/ Ω
75% RH
0
10k
20k
30k
40k
50k
Z'/ Ω

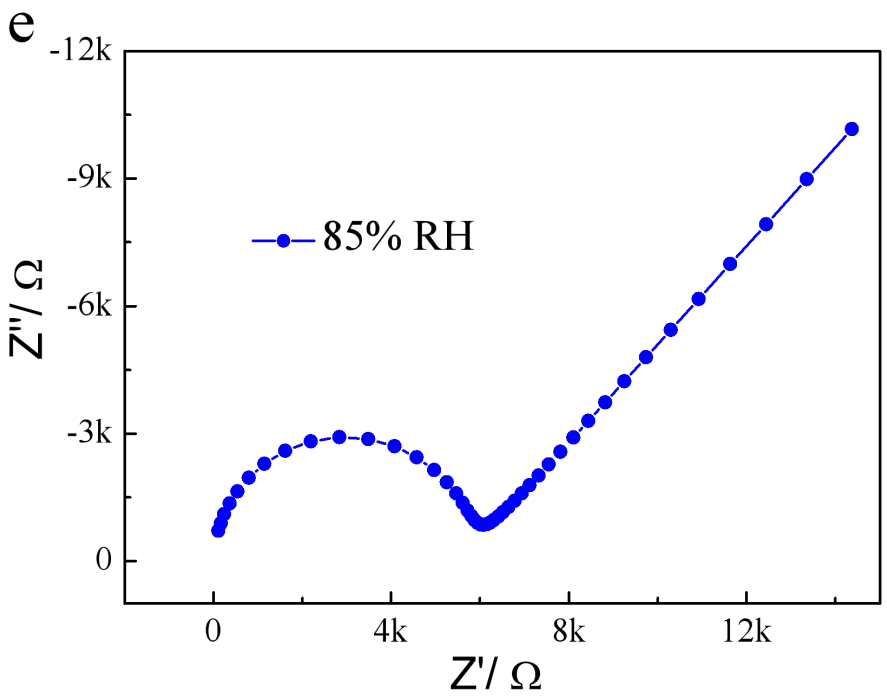

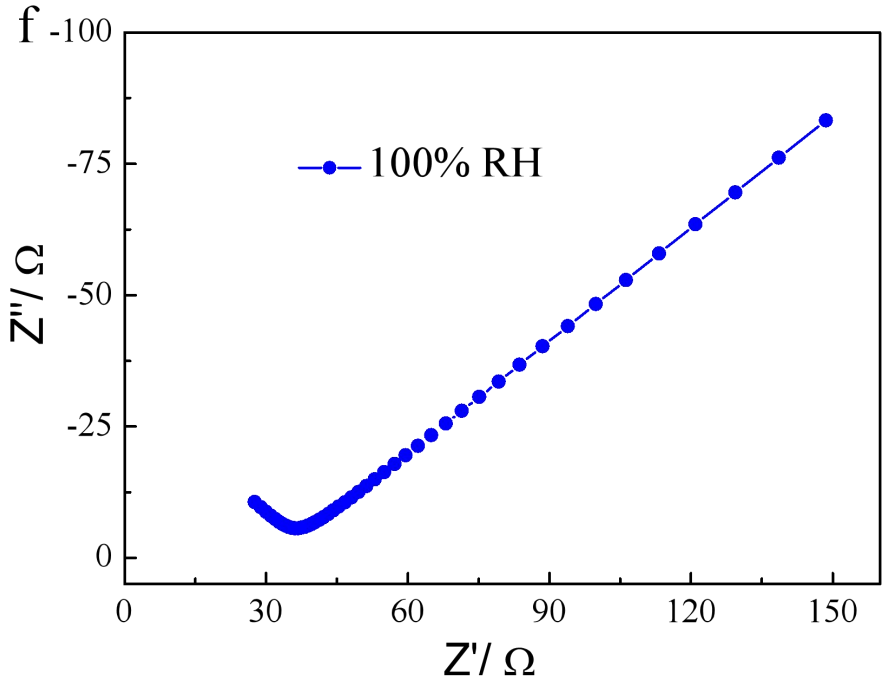

Supplementary Figure 15. Nyquist plots of FM-MOF-3 at (a) 33% RH, (b) 53% RH, (c) 65% RH, (d) 75% RH, (e) 85% RH and (f) 100% RH under room temperature.

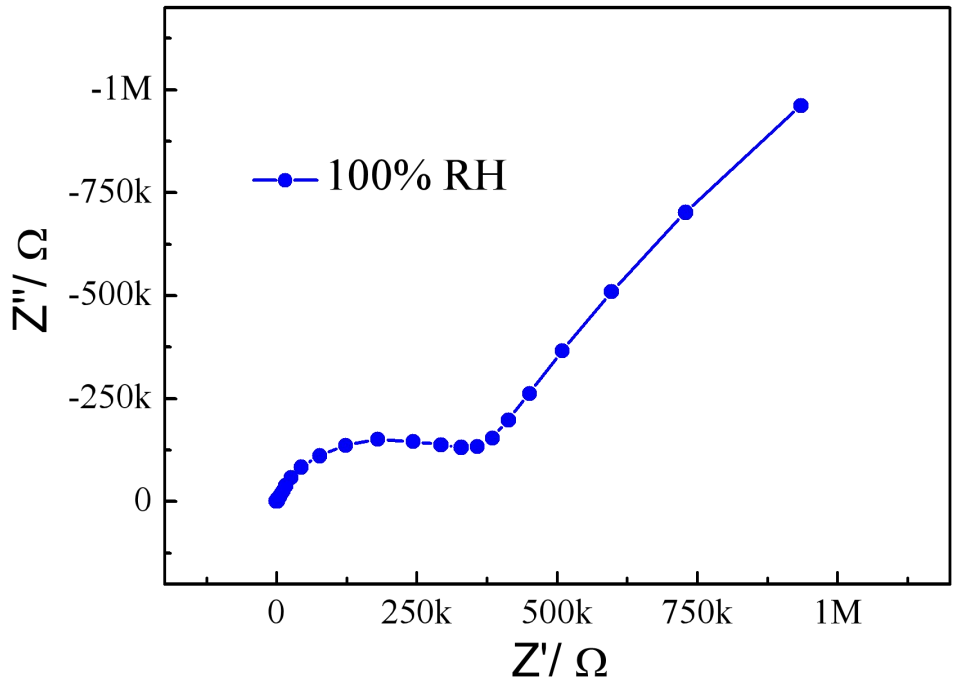

Supplementary Figure 16. Nyquist plots of MOF-808 at 100% RH under room temperature.

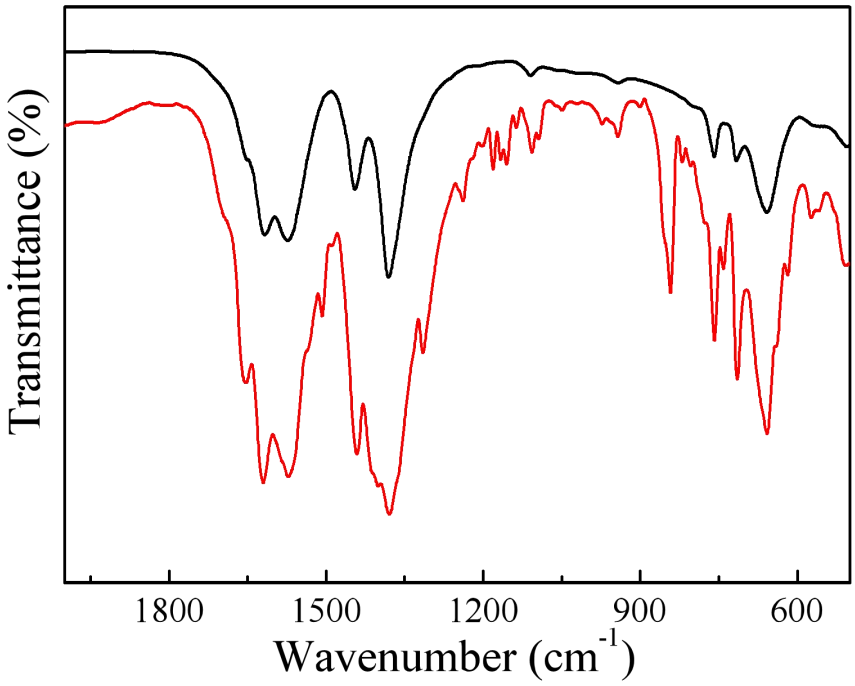

Supplementary Figure 17. FT-IR spectra of MOF-808 (black) and FM-MOF-4 (red).

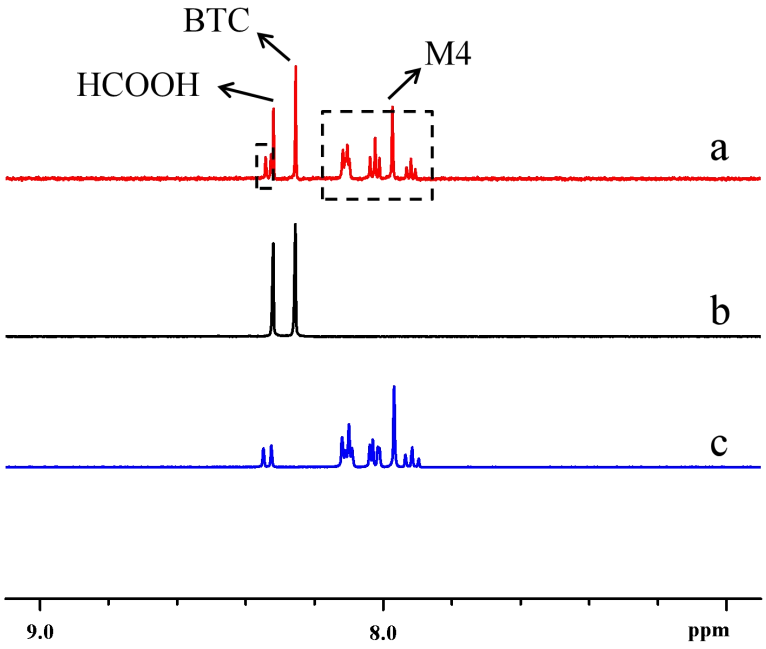

Supplementary Figure 18. ^{1}H NMR spectra of (a) alkaline-digested FM-MOF-4, (b) MOF-808, and (c) M4 (1-pyrenecarboxylic acid) in KOH/D_2O solution. It is obvious that the peak at 8.34 ppm for the hydrogen of the formate group in FM-MOF-4 decreases and new peaks around 7.8-8.4 ppm emerge, indicating the formate ligands on Zr_6 clusters in MOF-808 have been successfully substituted by M4.

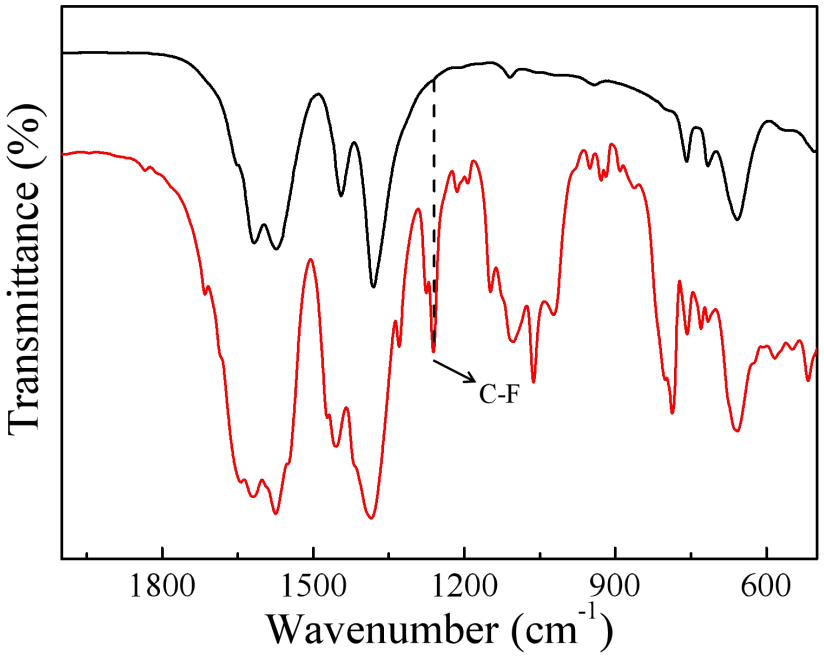

Supplementary Figure 19. FT-IR spectra of MOF-808 (black) and FM-MOF-5 (red). FM-MOF-5 exhibits a new peak at 1262 cm^{-1}, which is attributed to the stretching frequency of C-F in M5 (perfluorooctanoic acid).

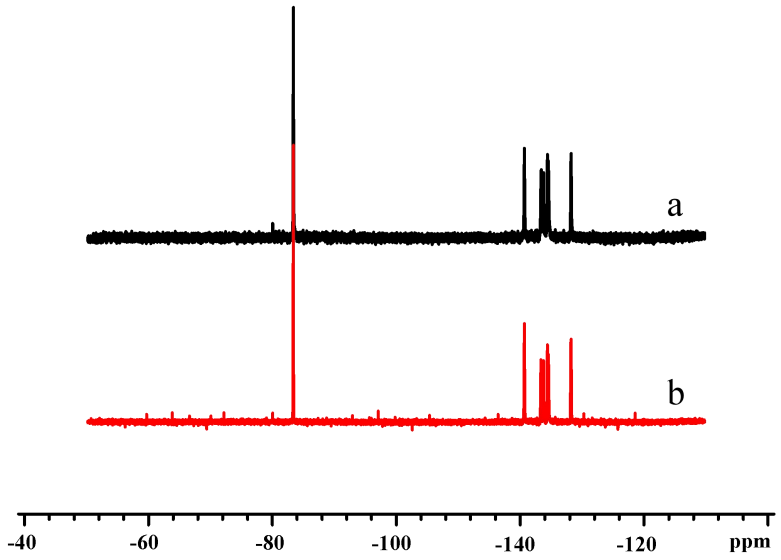

Supplementary Figure 20. ^{19}F NMR spectra of (a) acid-digested FM-MOF-5 and (b) M5 (perfluorooctanoic acid) in D_2SO4/DMSO solution. It is obvious that the peaks for the fluorine signals in FM-MOF-5 are consistent with those in M5, indicating perfluorooctanoic acid has been successfully inserted into MOF-808.

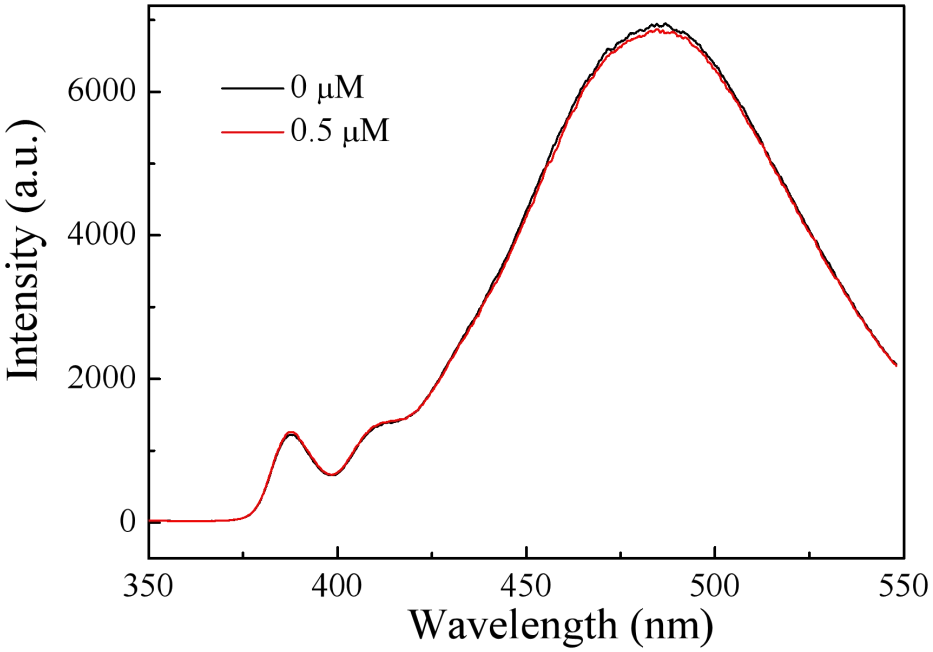

Supplementary Figure 21. Reduction in emission intensity of FM-MOF-4 upon addition of TNP solution in DMF.

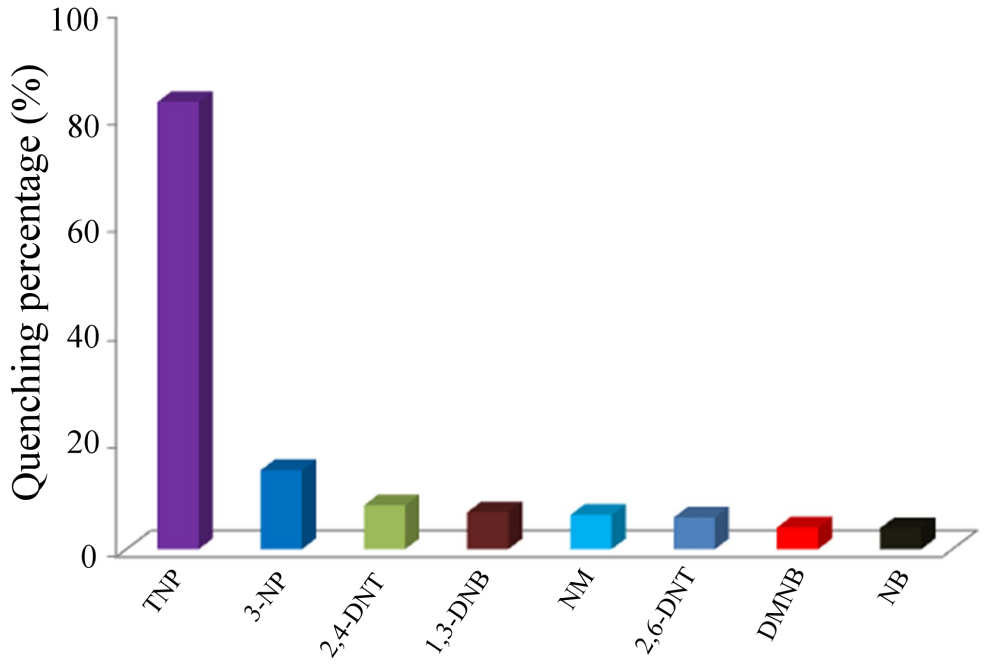

Supplementary Figure 22. Percentage of fluorescence quenching of FM-MOF-4 after addition of different explosive analytes (1 mM), including 3-Nitrophenol (3-NP), 2,4-dinitrotoluene (2,4-DNT), 1,3-dinitrobenzene (DNB), nitromethane (NM), 2,6-dinitrotoluene (2,6-DNT), 2,3-dimethyl- 2,3-dinitrobutane (DMNB) and nitrobenzene (NB).

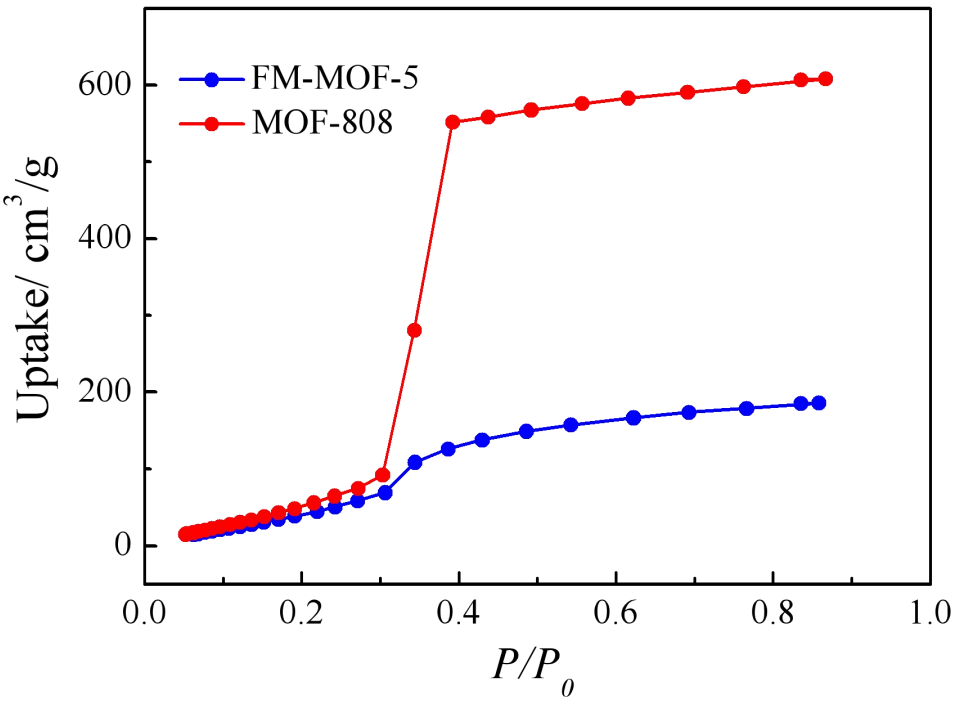

Supplementary Figure 23. Water adsorption isotherms of FM-MOF-5 and MOF-808 collected at 298 K.

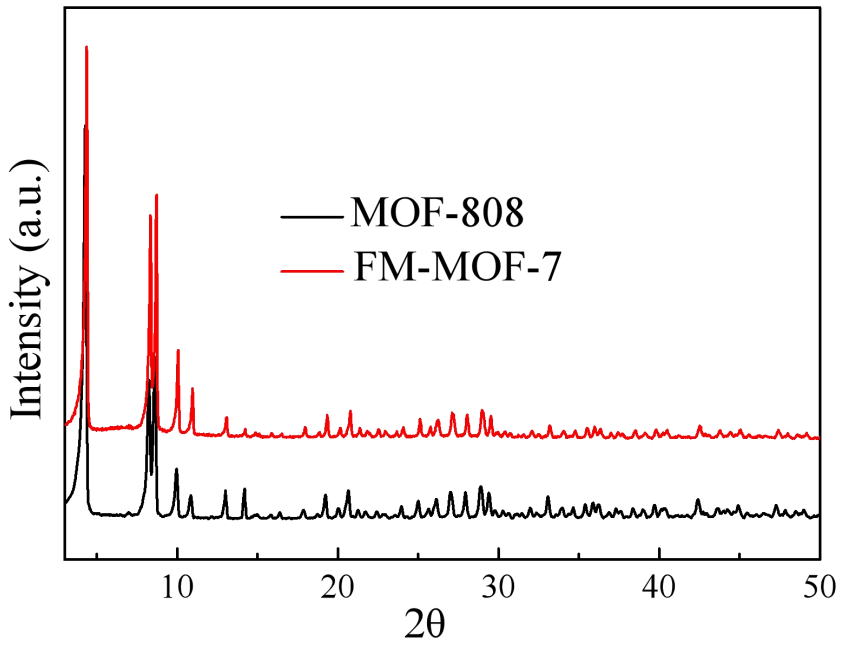

Supplementary Figure 24. PXRD patterns of FM-MOF-7 and MOF-808. The related peaks of FM-MOF-7 are in good agreement with those of pristine MOF-808, confirming that the crystal structure remains intact after M7 (propenoic acid) insertion.

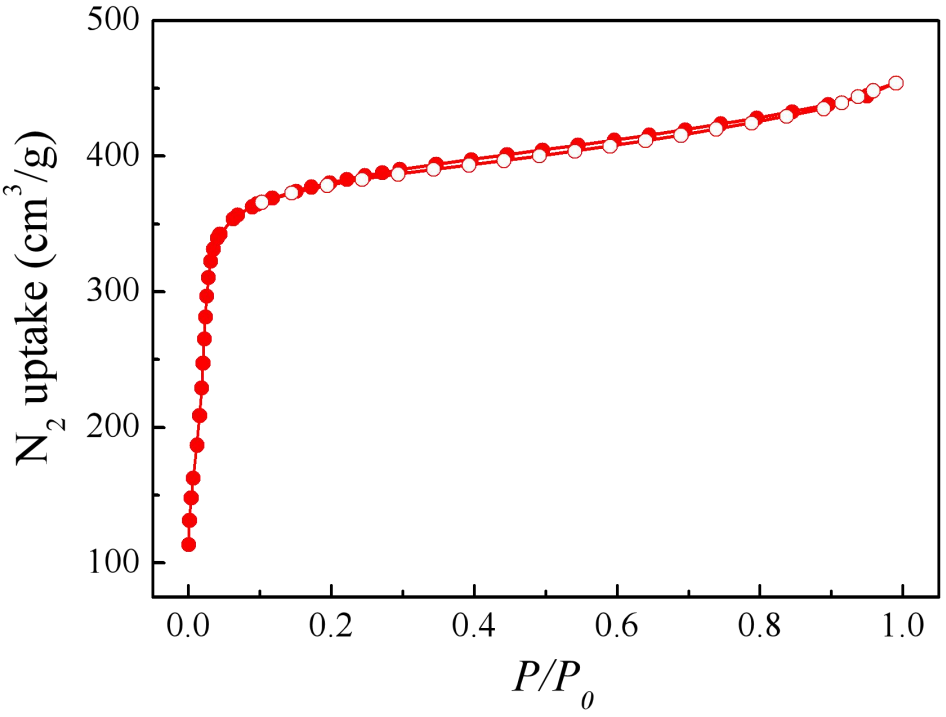

Supplementary Figure 25. N_2 adsorption-desorption isotherm of FM-MOF-7. The BET surface area of FM-MOF-7 was calculated to be 1612 m^2 g^{-1}.

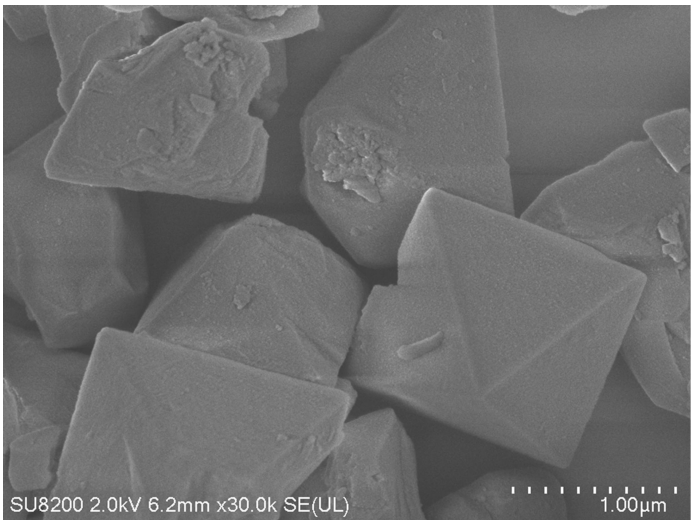

Supplementary Figure 26. SEM image of FM-MOF-7. It is obvious that FM-MOF-7 possesses octahedral morphology, indicating no apparent morphology change after M7 (propenoic acid) insertion.

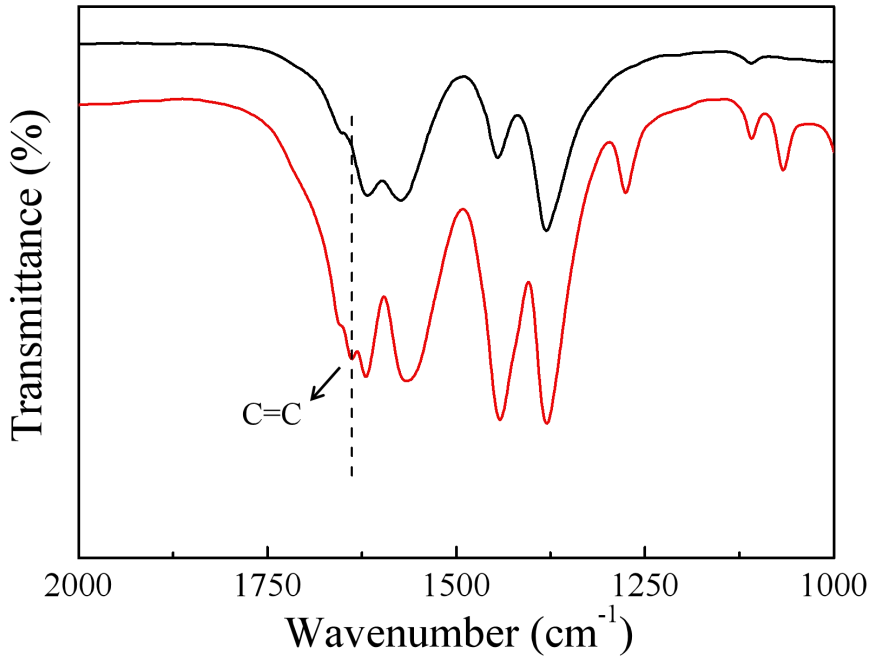

Supplementary Figure 27. FT-IR spectra of MOF-808 (black) and FM-MOF-7 (red).

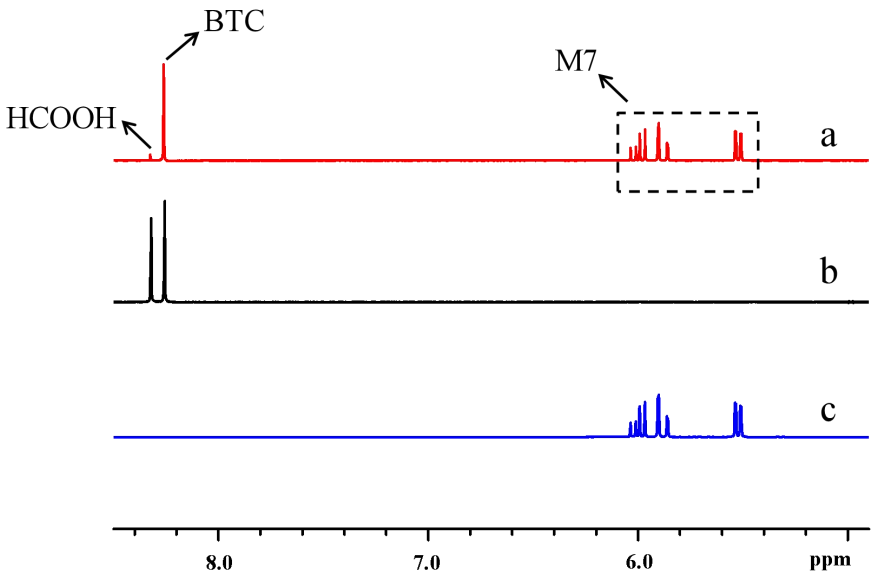

Supplementary Figure 28. ^{1}H NMR spectra of (a) alkaline-digested FM-MOF-7, (b) MOF-808, and (c) M7 (propenoic acid) in KOH/D_2O solution.

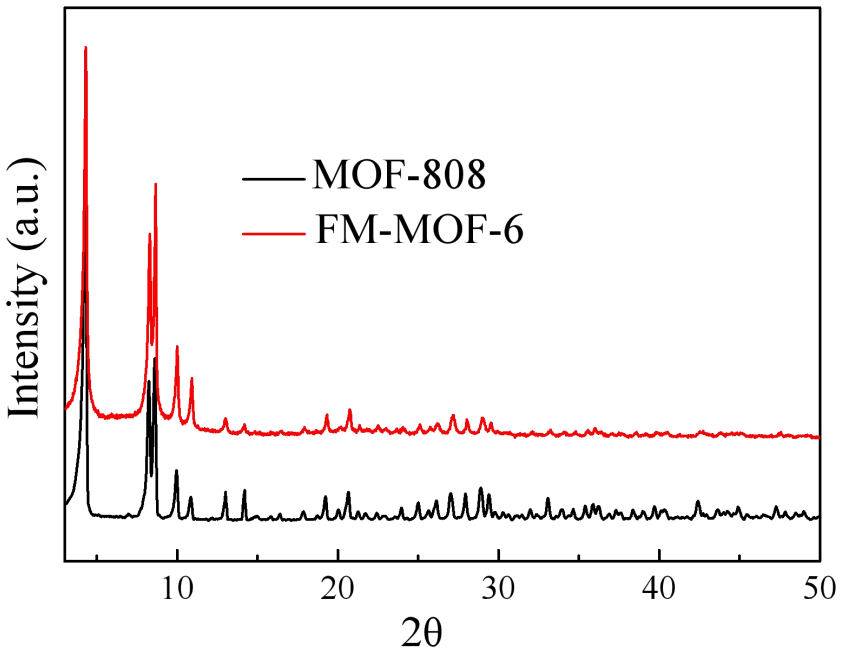

Supplementary Figure 29. PXRD patterns of FM-MOF-6 and MOF-808. The related peaks of FM-MOF-6 are in good agreement with those of pristine MOF-808, confirming that the crystal structure remains intact after such tandem postsynthetic modification.

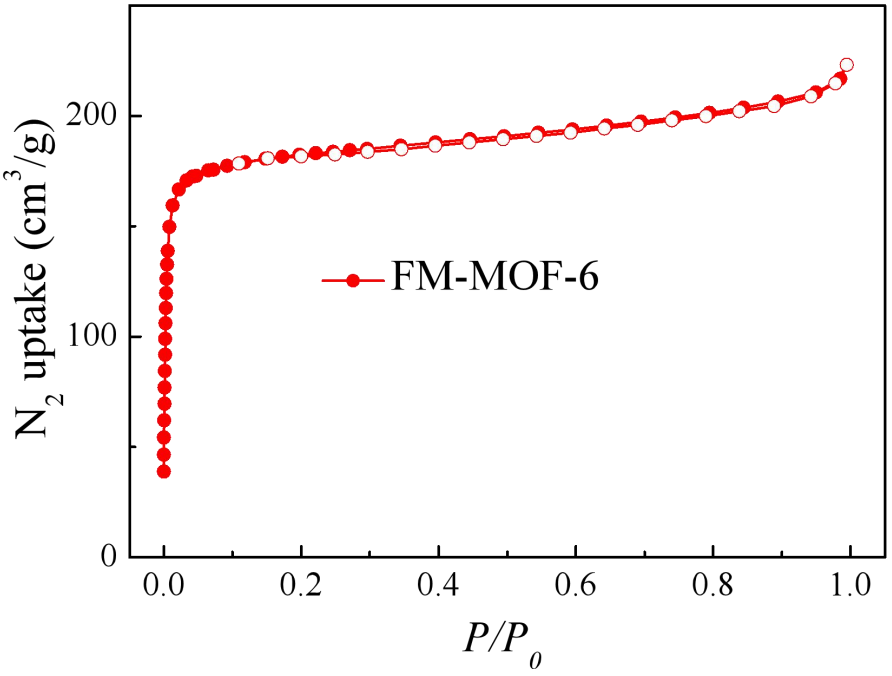

Supplementary Figure 30. N_2 adsorption-desorption isotherm of FM-MOF-6. The BET surface area of FM-MOF-6 was calculated to be 704 m^2 g^{-1}.

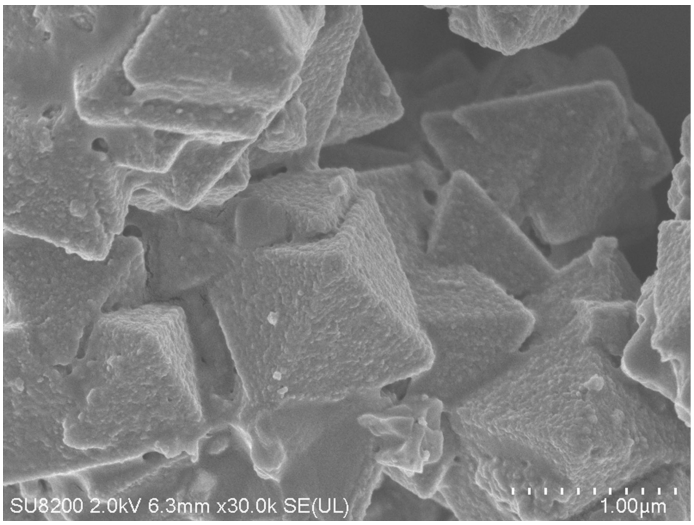

Supplementary Figure 31. SEM image of FM-MOF-6. Octahedral morphology was observed for FM-MOF-6.

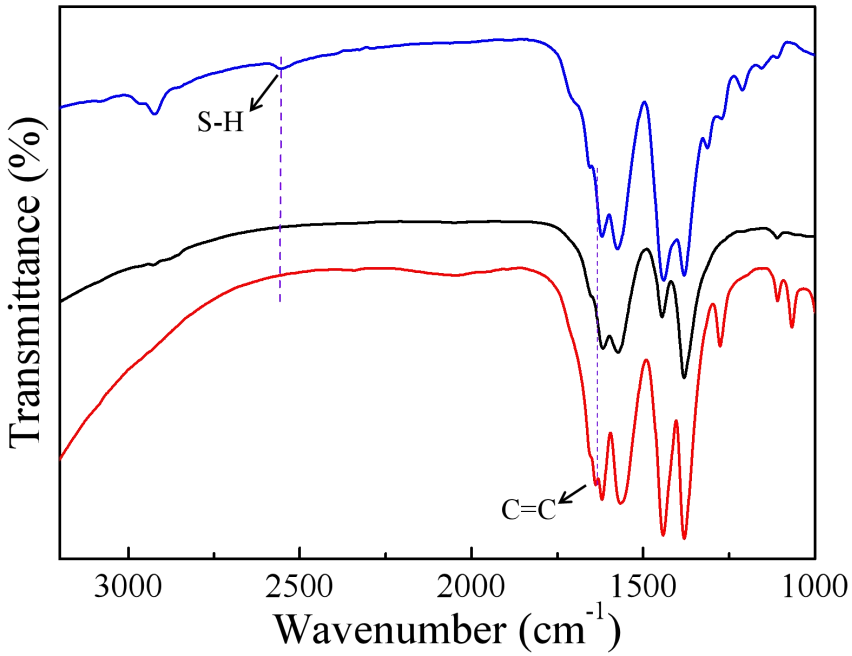

Supplementary Figure 32. FT-IR spectra of MOF-808 (black), FM-MOF-7 (red), and FM-MOF-6 (blue).

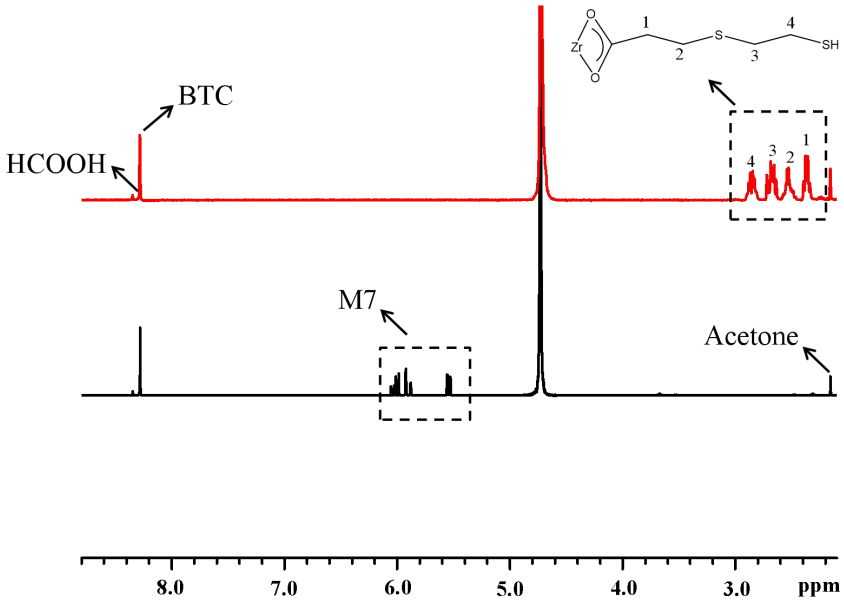

Supplementary Figure 33. ^{1}H NMR spectra of alkaline-digested FM-MOF-6 (red) and FM-MOF-7 (black) in KOH/D_2O solution.

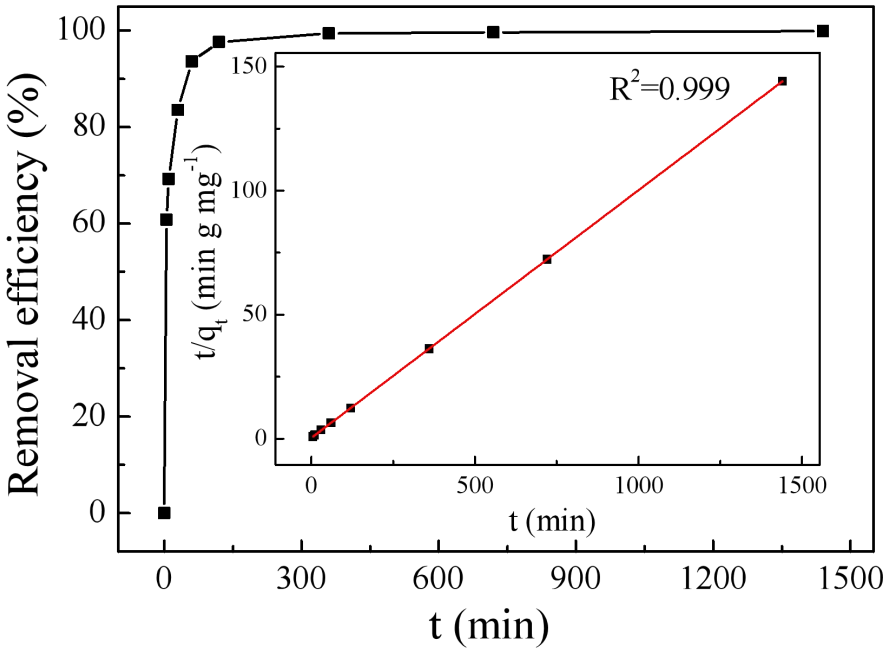

Supplementary Figure 34. Kinetics investigation of FM-MOF-6 for Hg^{2+} adsorption. Inset shows the pseudo-second-order kinetic plot for the adsorption.

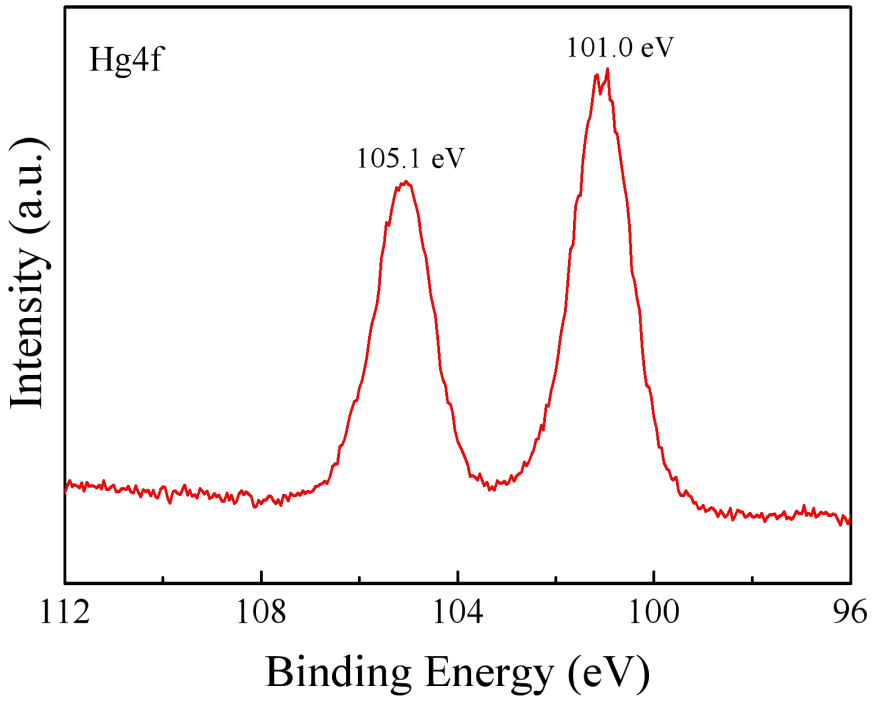

Supplementary Figure 35. Hg 4f XPS spectra of Hg^{2+}@FM-MOF-6.

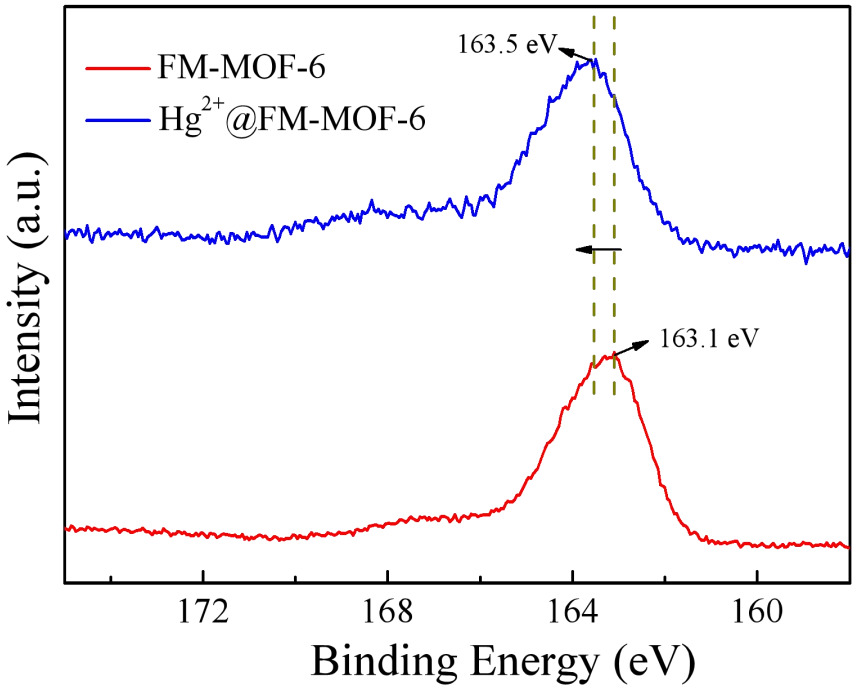

Supplementary Figure 36. S2p XPS spectra of FM-MOF-6 before and after Hg^{2+} loading.

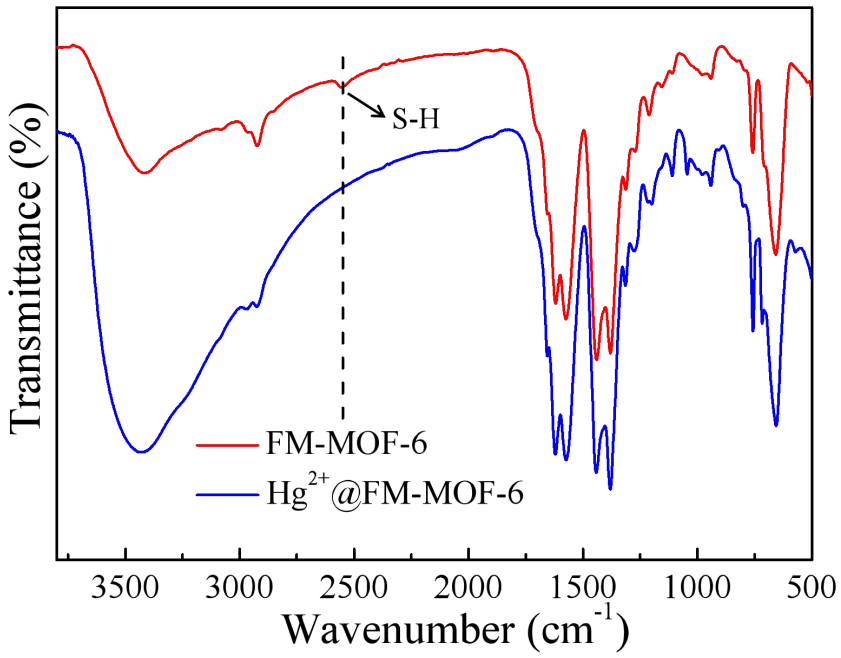

Supplementary Figure 37. FT-IR spectra of FM-MOF-6 before and after Hg^{2+} loading.

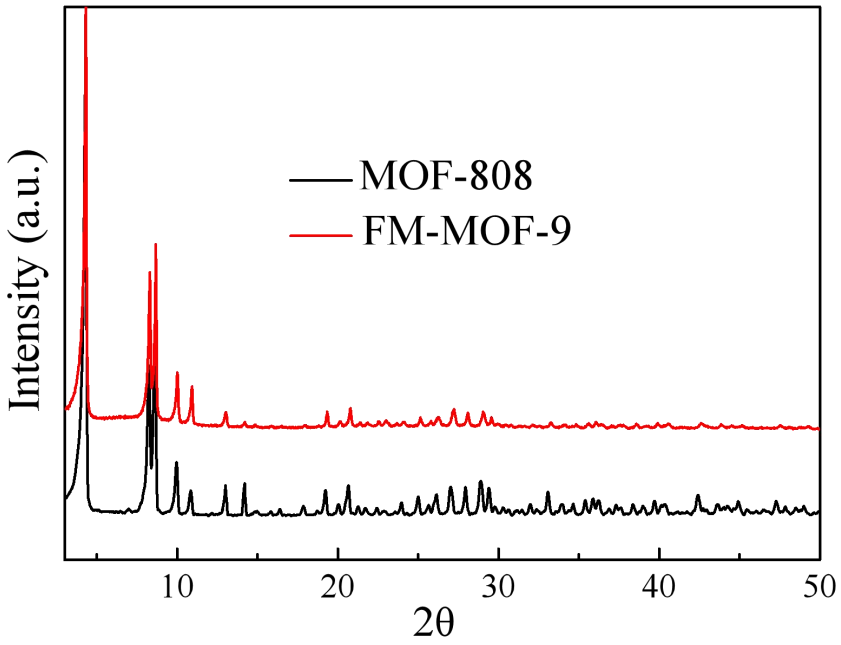

Supplementary Figure 38. PXRD patterns of FM-MOF-9 and MOF-808. The related peaks of FM-MOF-9 are in good agreement with those of pristine MOF-808, confirming that the crystal structure remains intact after M9 (bromoacetic acid) insertion.

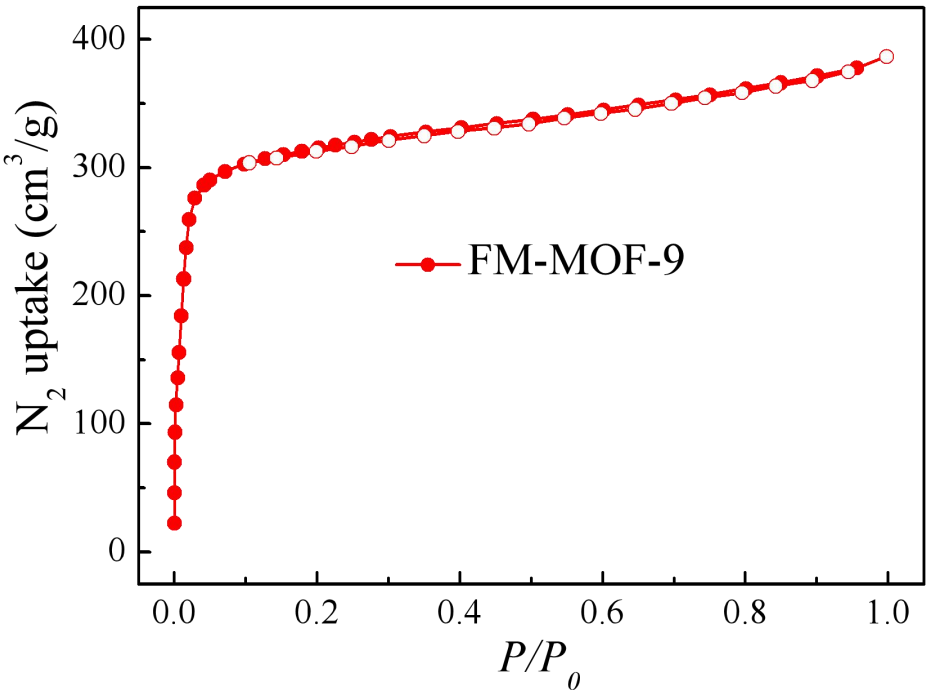

Supplementary Figure 39. N_2 adsorption-desorption isotherm of FM-MOF-9. The BET surface area of FM-MOF-9 was calculated to be 1325 m^2 g^{-1}.

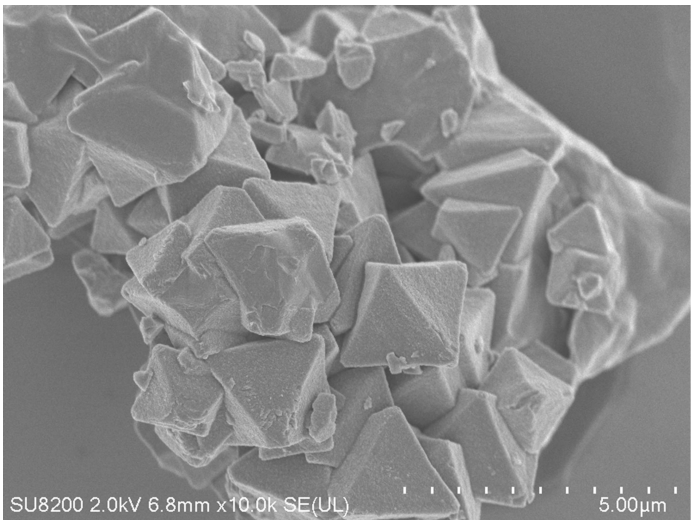

Supplementary Figure 40. SEM image of FM-MOF-9. Octahedral morphology was observed for FM-MOF-9.

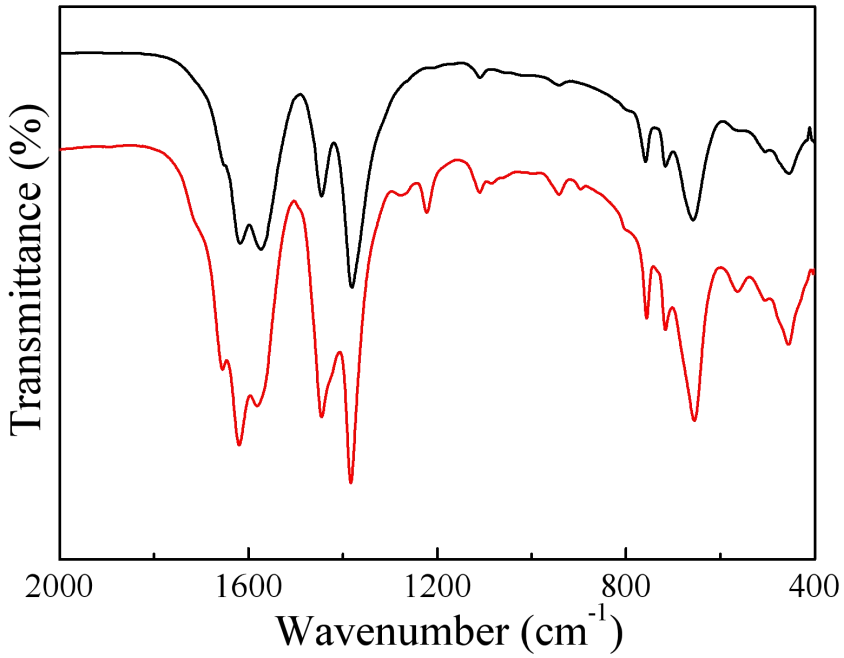

Supplementary Figure 41. FT-IR spectra of MOF-808 (black) and FM-MOF-9 (red).

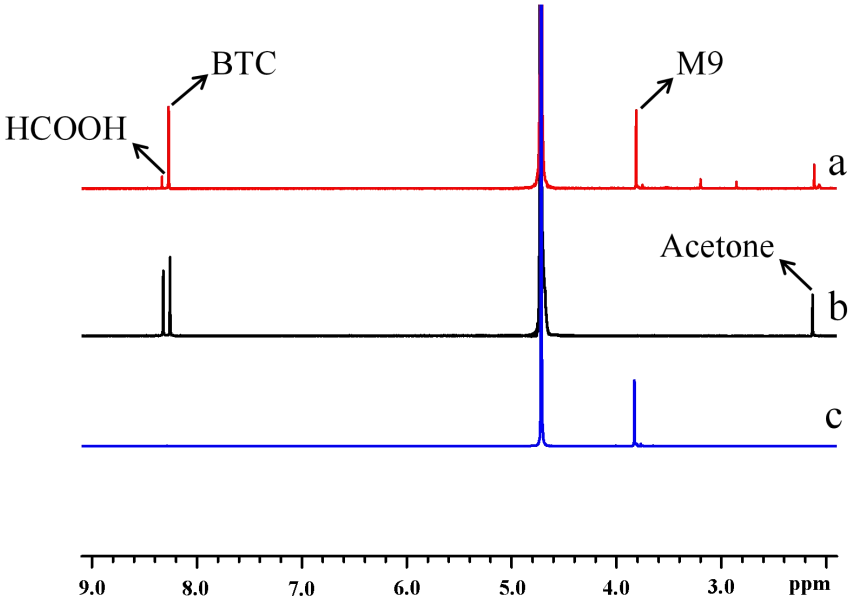

Supplementary Figure 42. ^{1}H NMR spectra of (a) alkaline-digested FM-MOF-9, (b) MOF-808, and (c) M9 (bromoacetic acid) in KOH/D_2O solution. It is obvious that the peak at 8.34 ppm for the hydrogen of the formate group in FM-MOF-9 decreases significantly and a new peak at 3.8 ppm corresponding to the hydrogen of -CH_2- in M9 emerges, indicating the formate ligands on Zr_6 clusters in MOF-808 have been successfully substituted by M9.

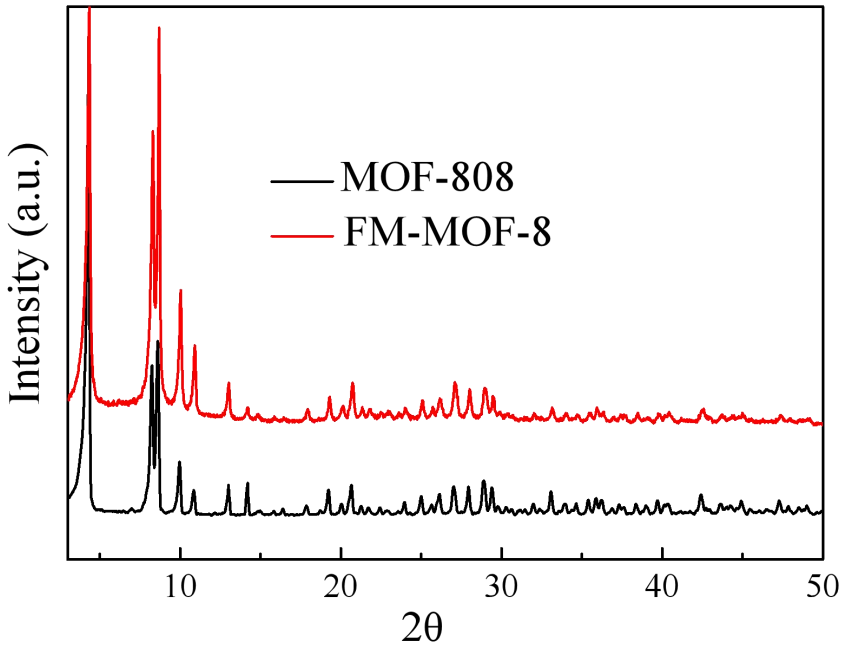

Supplementary Figure 43. PXRD patterns of FM-MOF-8 and MOF-808. The related peaks of FM-MOF-8 are in good agreement with those of pristine MOF-808, confirming that the crystal structure remains intact after such tandem postsynthetic modification.

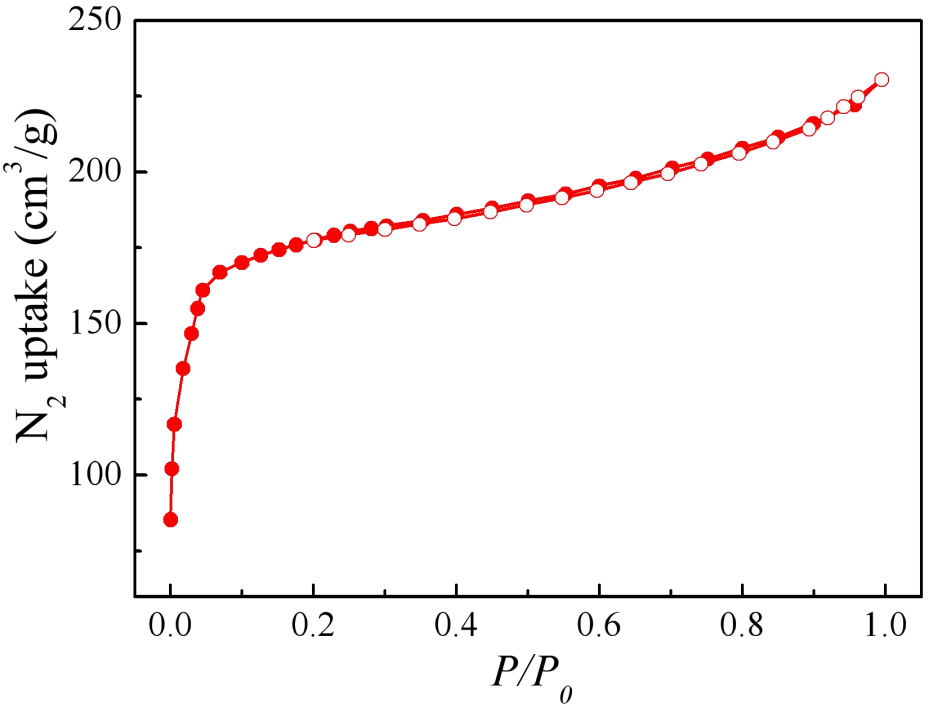

Supplementary Figure 44. N_2 adsorption-desorption isotherm of FM-MOF-8. The BET surface area of FM-MOF-8 was calculated to be 756 m^2 g^{-1}.

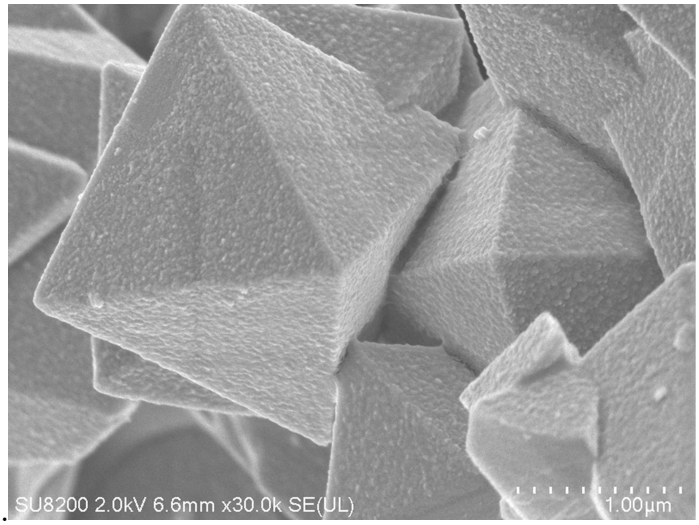

Supplementary Figure 45. SEM image of FM-MOF-8. Octahedral morphology was observed for FM-MOF-8, indicating no apparent morphology change after such tandem postsynthetic modification.

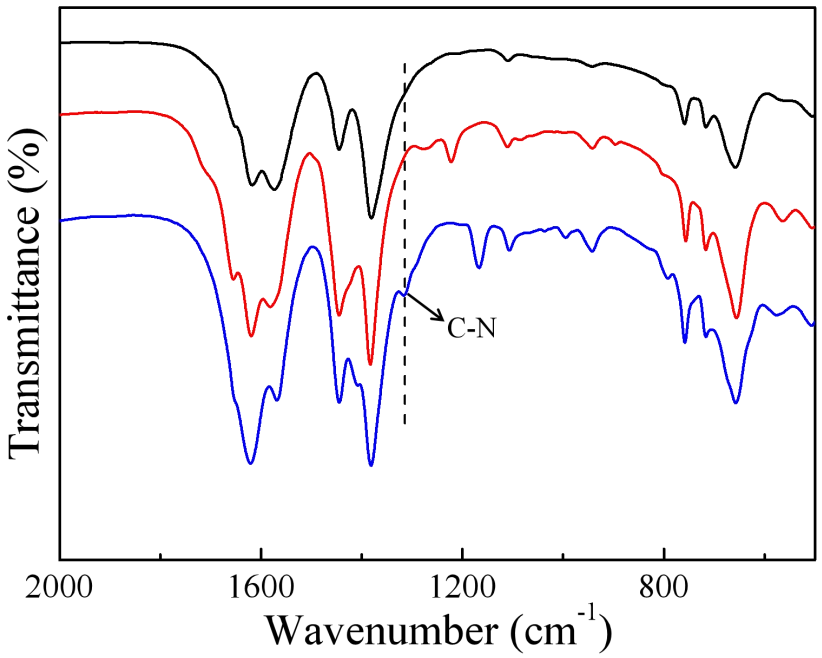

Supplementary Figure 46. FT-IR spectra of MOF-808 (black), FM-MOF-9 (red), and FM-MOF-8 (blue). In contrast with MOF-808 and FM-MOF-9, a new peak at 1316 cm^{-1} emerges, which can be ascribed to the stretching frequency of C-N in M8 (1-allylimidazole).

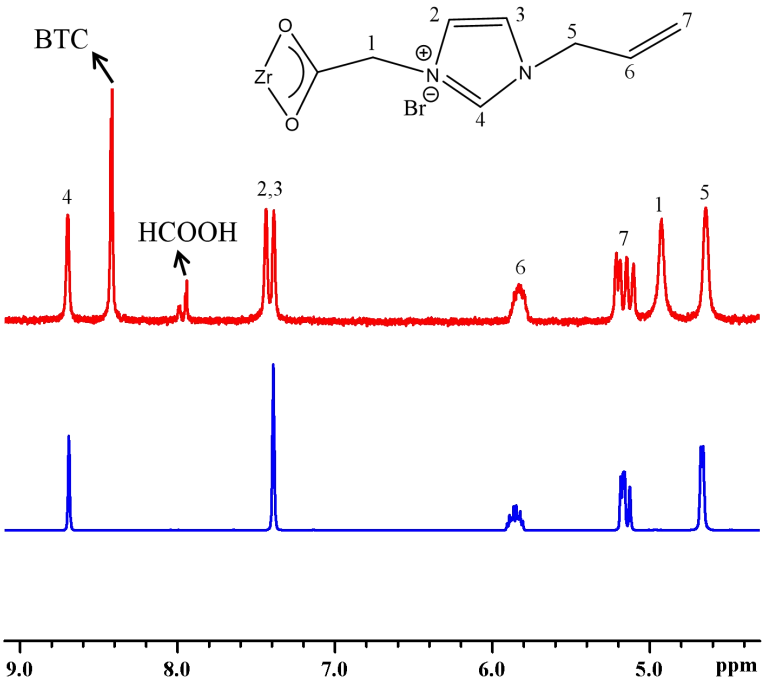

Supplementary Figure 47. ^{1}H NMR spectra of acid-digested FM-MOF-8 (red) and M8 (1-allylimidazole) in DMSO/D_2SO_4 solution. It is obvious that several new peaks attributed to the hydrogen signals of M8 emerge in FM-MOF-8, indicating the successful insertion of M8 into MOF-808 through such tandem postsynthetic modification.

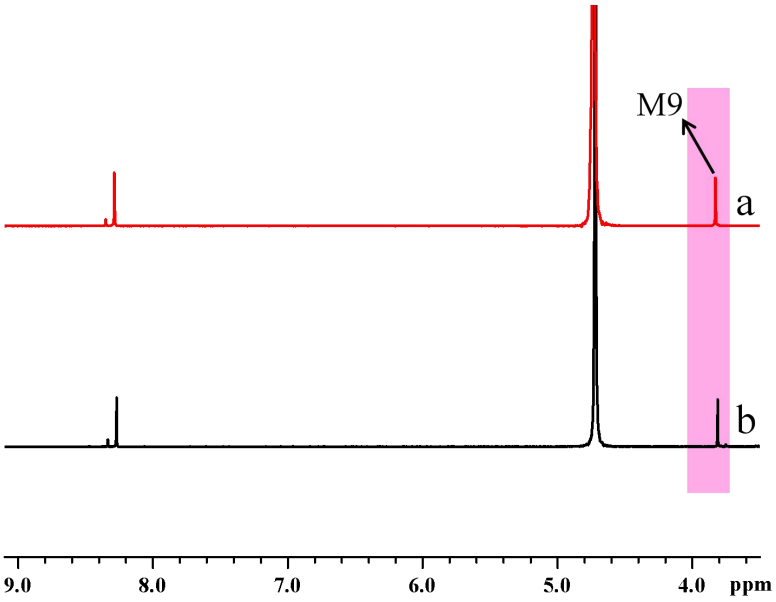

Supplementary Figure 48. ^{1}H NMR spectra of (a) as-transformed FM-MOF-9 from FM-MOF-2 and (b) FM-MOF-9 in KOH/D_2O solution.

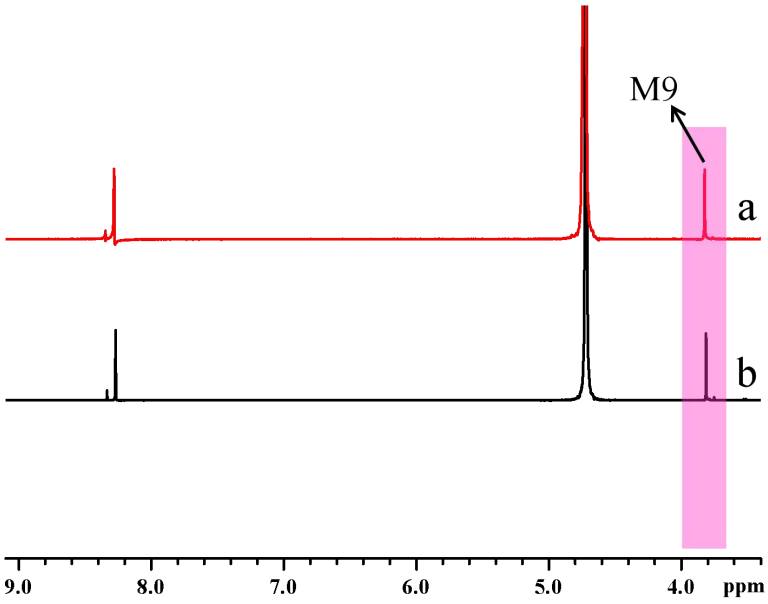

Supplementary Figure 49. ^{1}H NMR spectra of (a) as-transformed FM-MOF-9 from FM-MOF-7 and (b) FM-MOF-9 in KOH/D_2O solution.

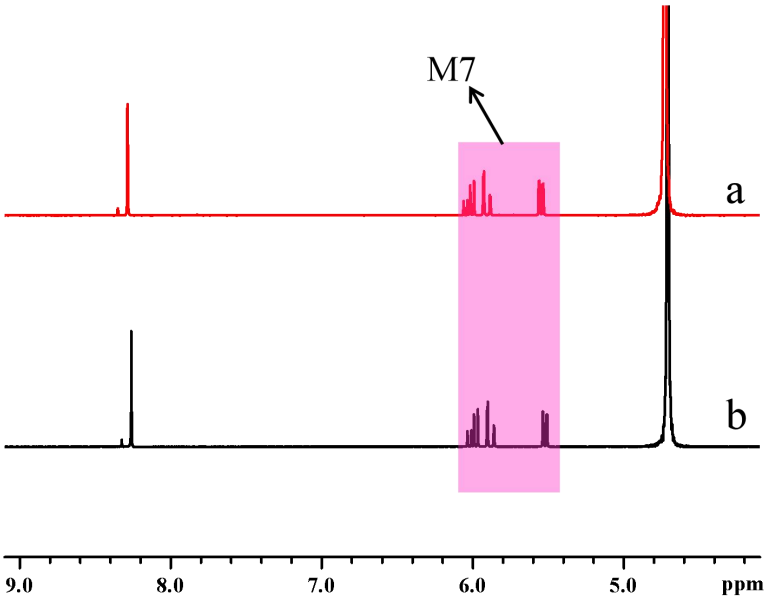

Supplementary Figure 50. ^{1}H NMR spectra of (a) as-transformed FM-MOF-7 from FM-MOF-2 and (b) FM-MOF-7 in KOH/D_2O solution.

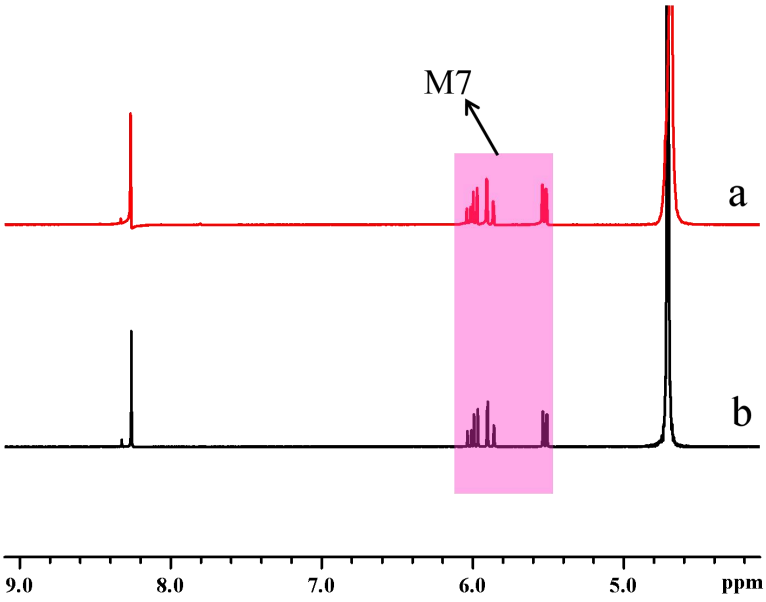

Supplementary Figure 51. ^{1}H NMR spectra of (a) as-transformed FM-MOF-7 from FM-MOF-9 and (b) FM-MOF-7 in KOH/D_2O solution.

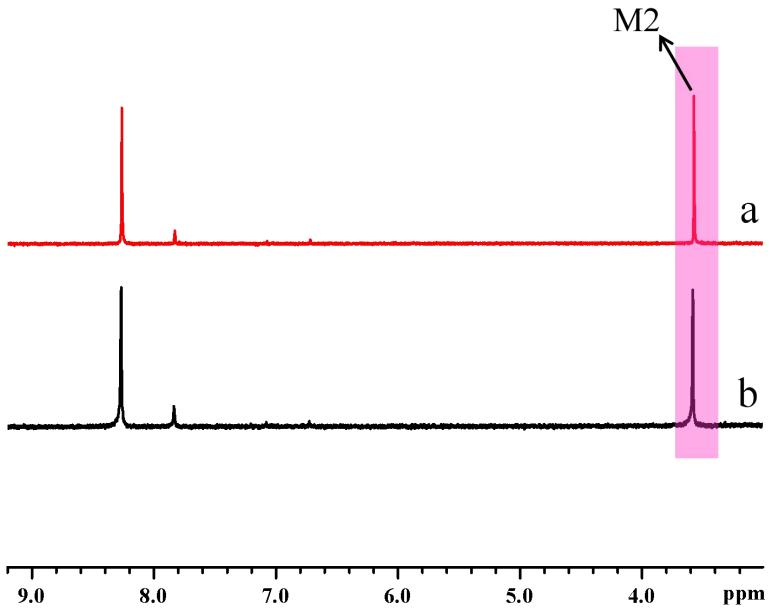

Supplementary Figure 52. ^{1}H NMR spectra of (a) as-transformed FM-MOF-2 from FM-MOF-9 and (b) FM-MOF-2 in D_2SO_4/DMSO solution.

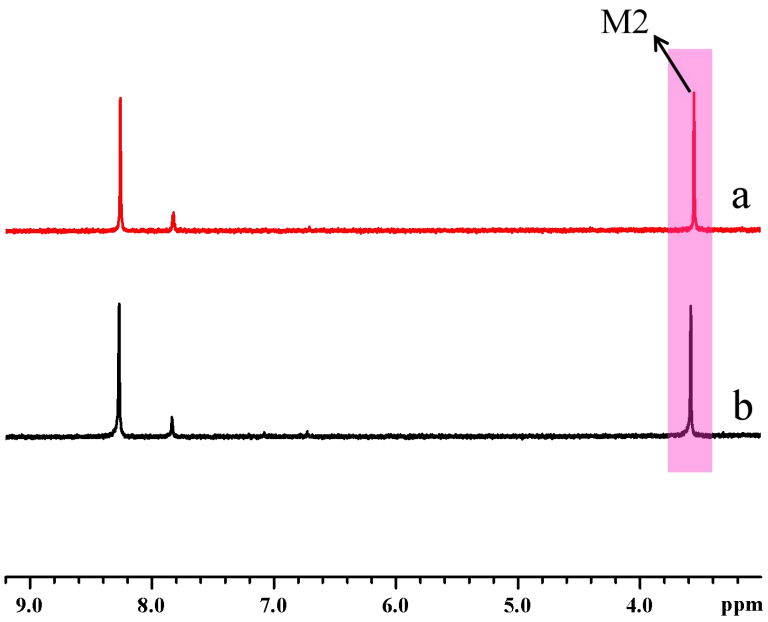

Supplementary Figure 53. ^{1}H NMR spectra of (a) as-transformed FM-MOF-2 from FM-MOF-7 and (b) FM-MOF-2 in D_2SO_4/DMSO solution.

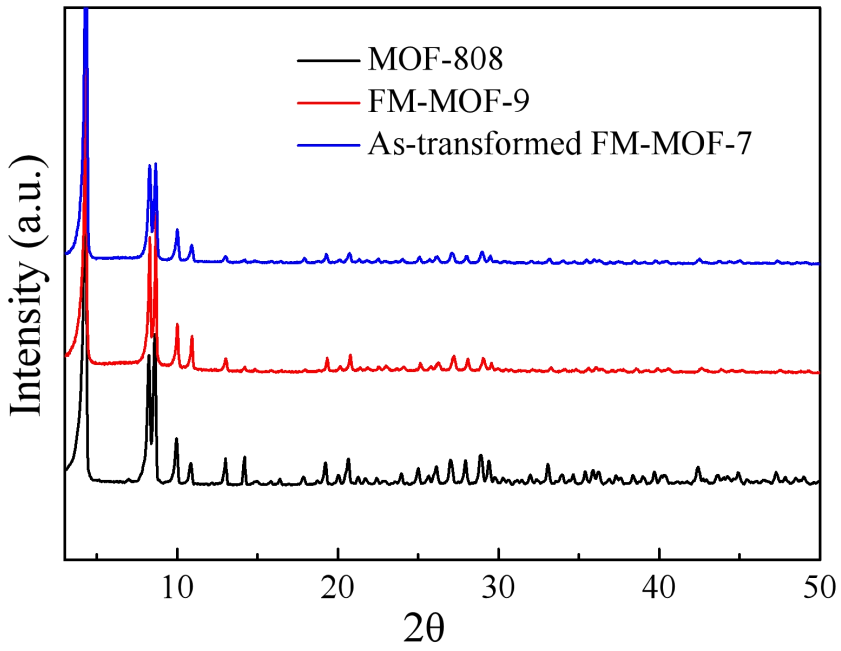

Supplementary Figure 54. PXRD patterns of MOF-808, as-transformed FM-MOF-7 from FM-MOF-9 and parent FM-MOF-9.

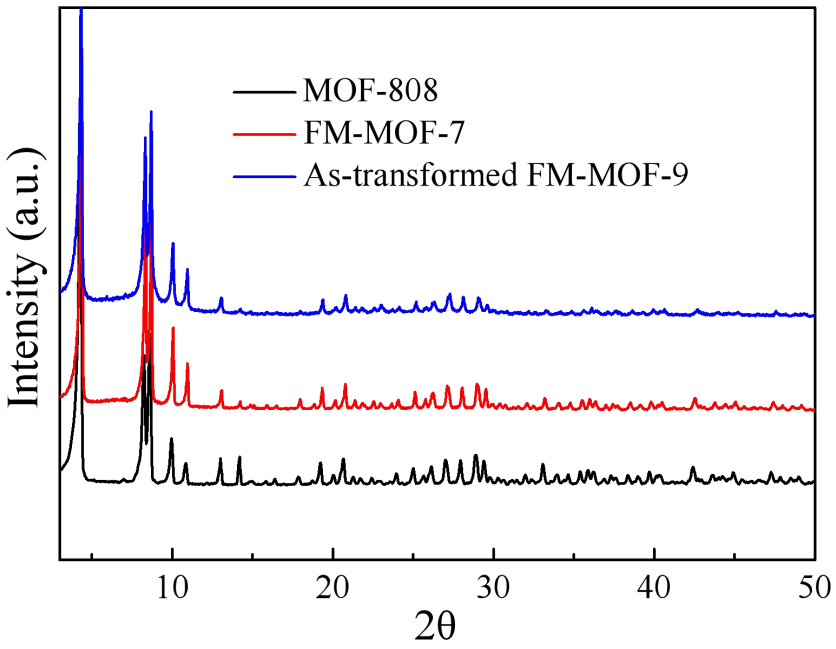

Supplementary Figure 55. PXRD patterns of MOF-808, as-transformed FM-MOF-9 from FM-MOF-7 and parent FM-MOF-7.

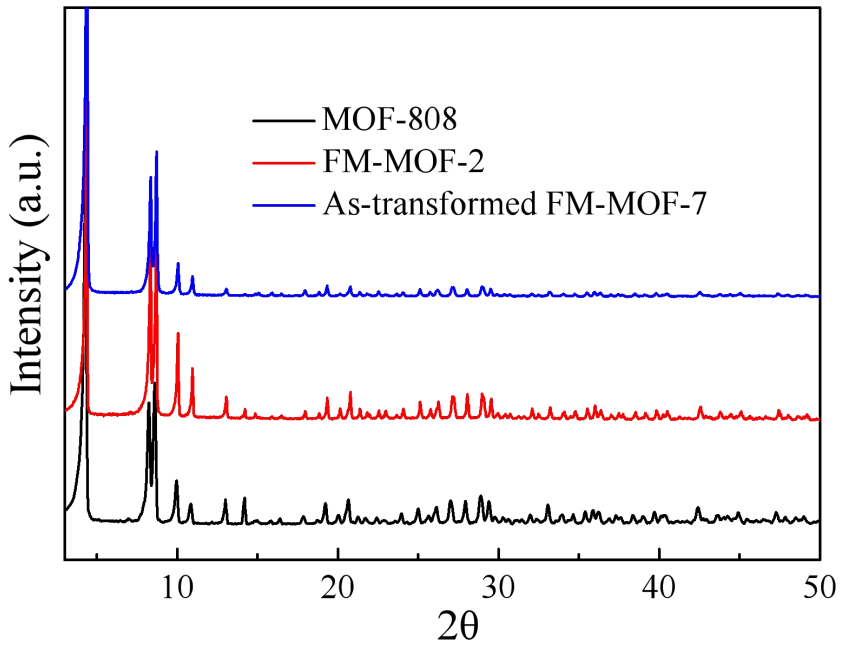

Supplementary Figure 56. PXRD patterns of MOF-808, as-transformed FM-MOF-7 from FM-MOF-2 and parent FM-MOF-2.

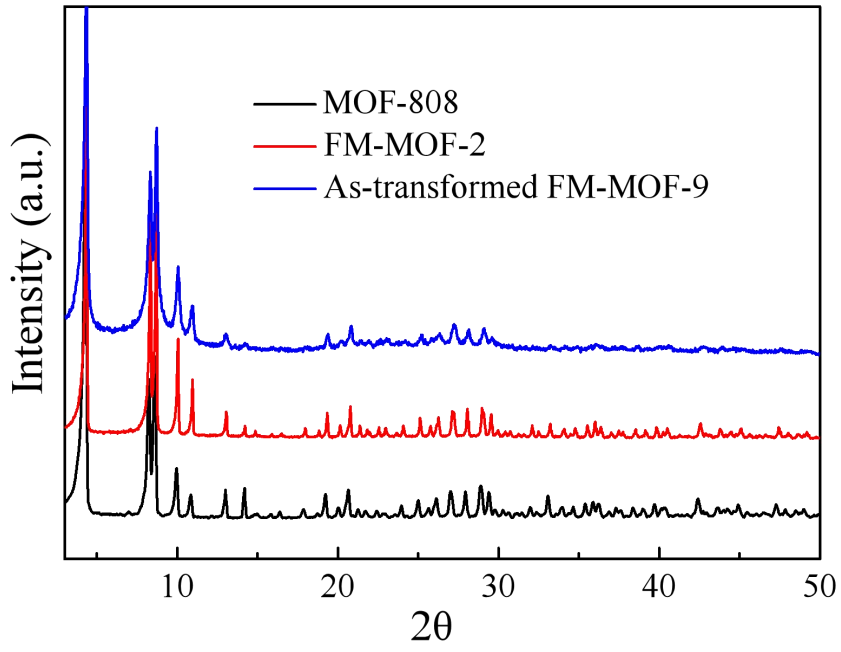

Supplementary Figure 57. PXRD patterns of MOF-808, as-transformed FM-MOF-9 from FM-MOF-2 and parent FM-MOF-2.

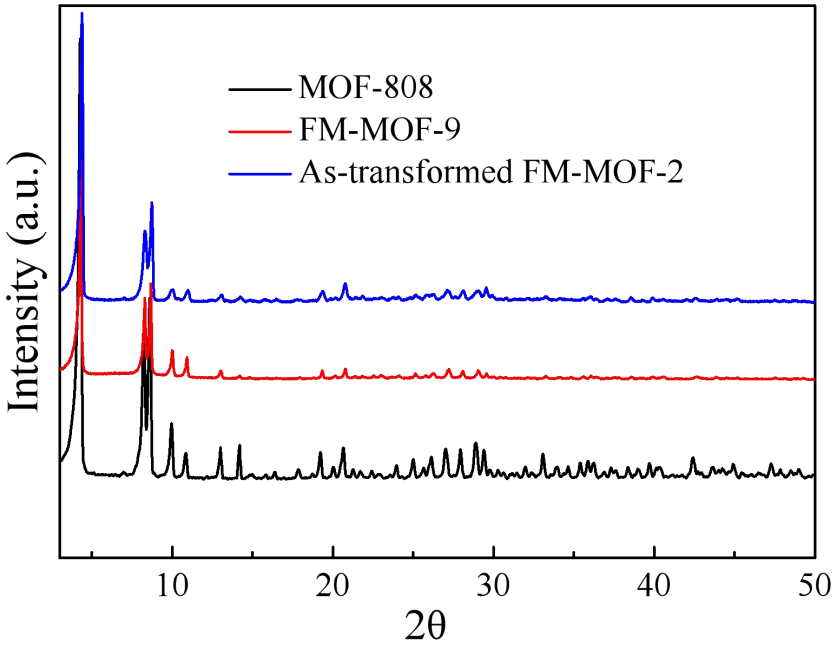

Supplementary Figure 58. PXRD patterns of MOF-808, as-transformed FM-MOF-2 from FM-MOF-9 and parent FM-MOF-9.

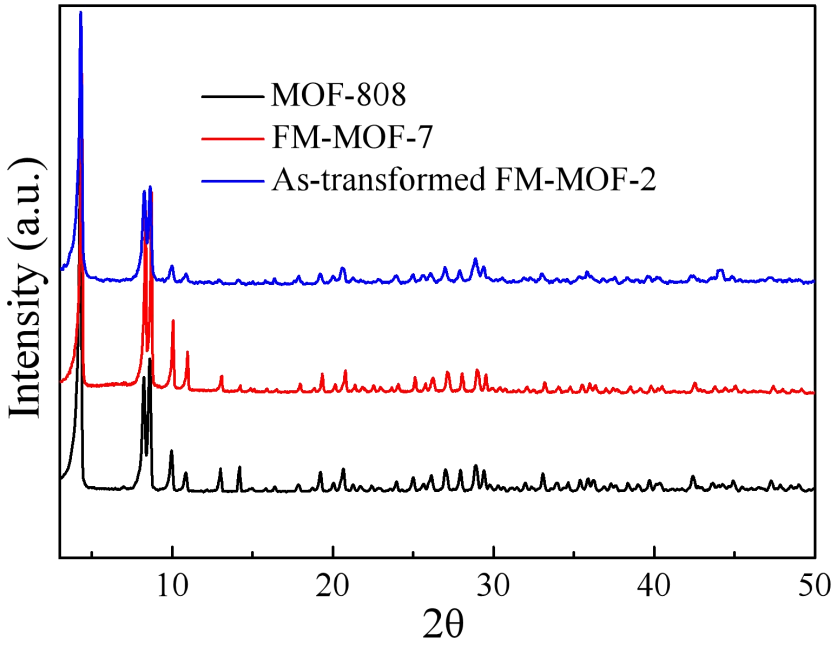

Supplementary Figure 59. PXRD patterns of MOF-808, as-transformed FM-MOF-2 from FM-MOF-7 and parent FM-MOF-7.

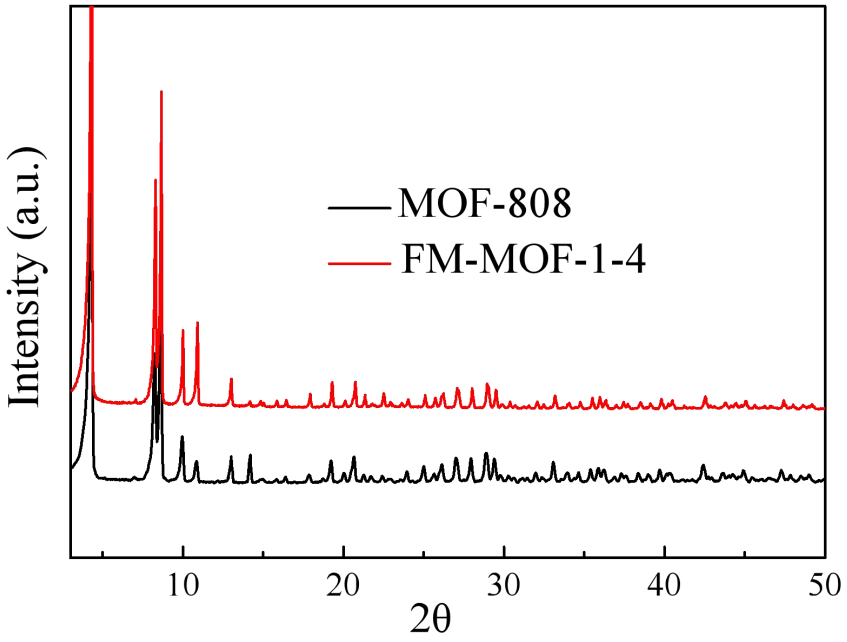

Supplementary Figure 60. PXRD patterns of MOF-808 and FM-MOF-1-4. The related peaks of FM-MOF-1-4 are in good agreement with those of pristine MOF-808, confirming that the crystal structure remains intact after modification.

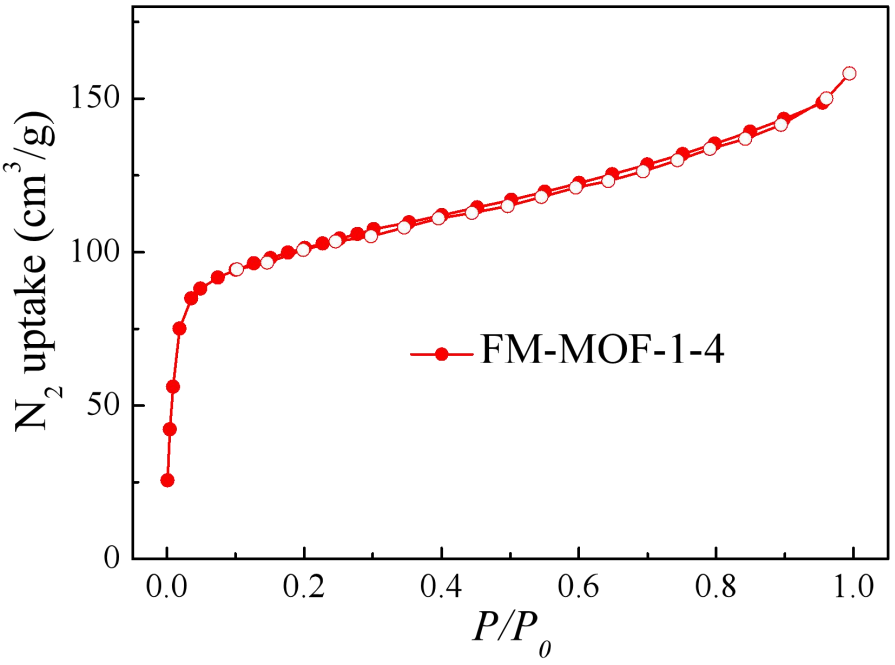

Supplementary Figure 61. N_2 adsorption-desorption isotherm of FM-MOF-1-4. The BET surface area of FM-MOF-1-4 was calculated to be 344 m^2 g^{-1}.

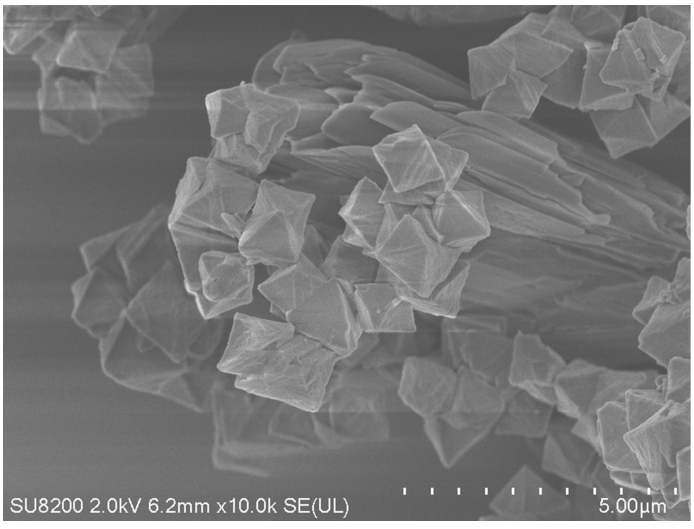

Supplementary Figure 62. SEM image of FM-MOF-1-4. Octahedral morphology was observed for FM-MOF-1-4.

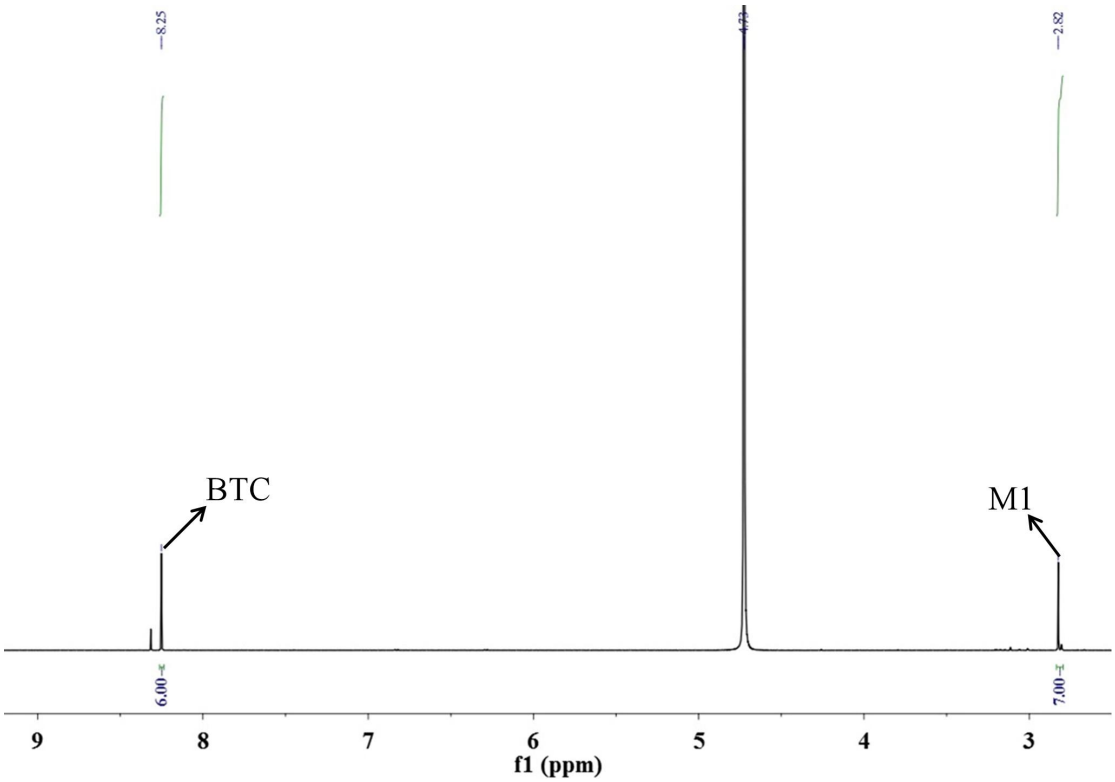

Supplementary Figure 63. ^{1}H NMR spectra of alkaline-digested FM-MOF-1 in KOH/D_2O solution after integral analysis.

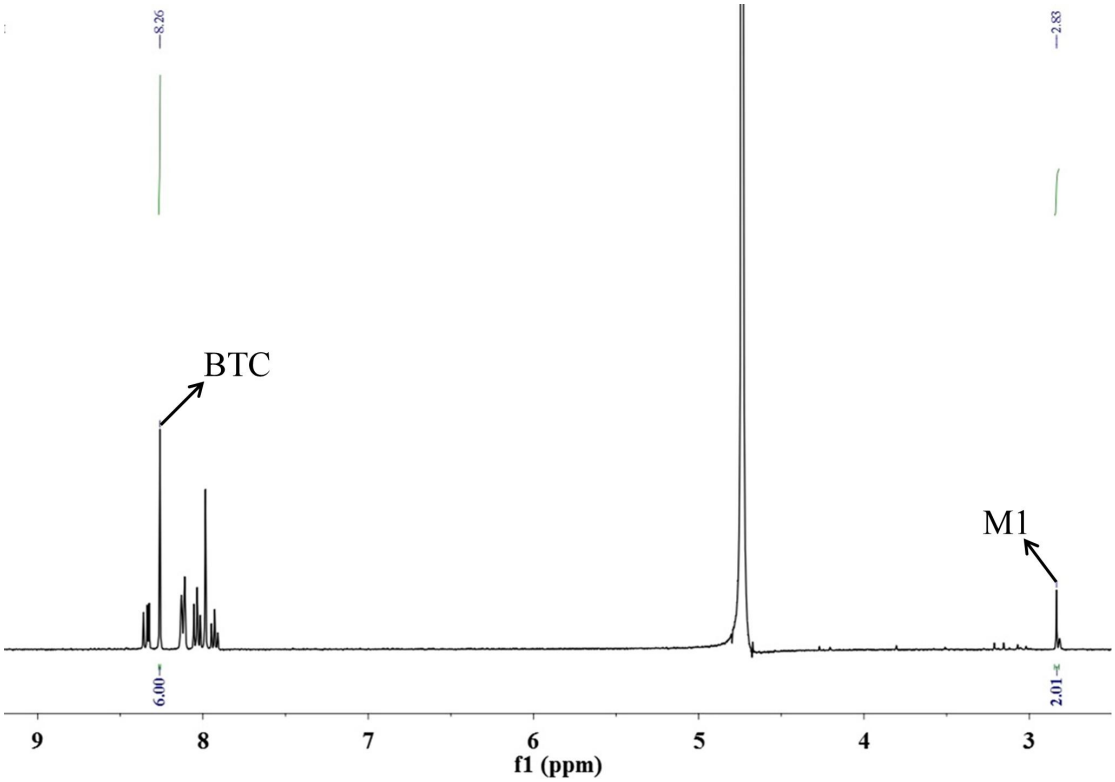

Supplementary Figure 64. ^{1}H NMR spectra of alkaline-digested FM-MOF-1-4 in KOH/D_2O solution after integral analysis.

Supplementary Table 1. Comparison of the maximum adsorption capacities of FM-MOF-2 for Ag^{+} with various porous materials

Adsorbents	Maximum adsorption capacity/ mg g^{-1}	Supplementary refs.
Ag-IISHPs	80.5	[1]
EBG	90.06	[2]
ITG-OCMC	156.32	[3]
F-WS_2 MCs	186.2	[4]
PP-g-GMA@MEA	262.51	[5]
KMS-2	408	[6]
MoS4-LDH	450	[7]
BBCF	600	[8]
N,S-CDs	714.3	[9]
PPy/MAA	714.28	[10]
FM-MOF-2	806	this work

Supplementary Table 2. Comparison of the maximum adsorption capacities of FM-MOF-6 for Hg^{2+} with various MOF-based materials

Adsorbents	Maximum adsorption capacity/ mg g^{-1}	Supplementary refs.
Zr-DMBD	197	[11]
Zr-M1	275	[12]
Zn(hip)-MOF	278	[13]
Cys-UIO-66	350.14	[14]
PCN-224 - MAA/MF	412.5	[15]
FJI-H12	439.8	[16]
In2S3@MIL-101	518.2	[17]
NENU-401	596.57	[18]
CoCNSP	716	[19]
BioMOF	900	[20]
TLMSM	954.7	[21]
FM-MOF-6	1077	this work

Experimental details

Characterization

PXRD patterns were collected on Bruker AXS D2 Phaser equipped with a Cu sealed tube (λ = 1.5418 Å) operating at 40 kV and 15 mA. The nitrogen adsorption-desorption isotherms of FM-MOFs were measured using Autosorb-IQ-MP (Quantachrome Instruments) at -196 °C. The scanning electron microscopy (SEM) images of FM-MOFs were obtained using a Hitachi SU8200 instrument. The IR spectra were measured with a Nicolet 6700 FTIR spectrophotometer. NMR spectra were determined on a Bruker Fourier 600M spectrometer. The XPS data were collected using an ESCALAB 250 X-ray photoelectron spectroscopy with Al Kα X-ray as the excitation source. The concentration of metal ions in aqueous solution was measured by an inductively coupled plasma-mass spectrometry (ICP-MS). The fluorescence data were measured by fluorescence spectrometer (F-7000).

Chemicals

Solvents were purified base on standard laboratory methods. Other reagents were used as received from commercial supplies without further purification.

Synthesis of FM-MOF-1

MOF-808 was prepared according to previous literature[22,23]. Then, the activated MOF-808 (0.100 g) was added to thioglycolic acid (2.5 ml) in a solution containing 10 ml of N,N-Dimethylformamide (DMF). The mixture was stirred and heated to 60°C for 24 h under N_2 atmosphere. The resultant precipitate was obtained by centrifugation, washed with DMF and acetone several times, and then dried at 60 °C overnight under vacuum condition to produce the solid of FM-MOF-1.

Synthesis of FM-MOF-2

The activated MOF-808 (0.100 g) was added to propiolic acid (2 ml) in a solution containing 10 ml of acetonitrile. The mixture was stirred and heated to 60°C for 24 h under N_2 atmosphere. The resultant precipitate was obtained by centrifugation, washed with DMF and acetone several times, and then dried at 60 °C overnight under vacuum condition to produce the solid of FM-MOF-2.

Synthesis of FM-MOF-3

The activated MOF-808 (0.100 g) was added to oxalic acid (0.900 g) in a solution containing 10 ml of DMF. The mixture was stirred and heated to 70°C for 24 h under N_2 atmosphere. The resultant precipitate was obtained by centrifugation, washed with DMF and acetone several times, and then dried at 60 °C overnight under vacuum condition to produce the solid of FM-MOF-3.

Synthesis of FM-MOF-4

The activated MOF-808 (0.100 g) was added to 1-pyrenecarboxylic acid (0.800 g) in a solution containing 10 ml of DMF. The mixture was stirred and heated to 60°C for 24 h under N_2 atmosphere. The resultant precipitate was obtained by centrifugation, washed with DMF and acetone several times, and then dried at 60 °C overnight under vacuum condition to produce the solid of FM-MOF-4.

Synthesis of FM-MOF-5

The activated MOF-808 (0.100 g) was added to perfluorooctanoic acid (0.400 g) in a solution containing 10 ml of DMF. The mixture was stirred and heated to 60°C for 24 h under N_2 atmosphere. The resultant precipitate was obtained by centrifugation, washed with DMF and acetone several times, and then dried at 60 °C overnight under vacuum condition to produce the solid of FM-MOF-5.

Synthesis of FM-MOF-7

The activated MOF-808 (0.100 g) was added to propenoic acid (2 ml) in a solution containing 10 ml of acetonitrile. The mixture was stirred and heated to 60°C for 24 h under N_2 atmosphere. The resultant precipitate was obtained by centrifugation, washed with DMF and acetone several times, and then dried at 60 °C overnight under vacuum condition to produce the solid of FM-MOF-7.

Synthesis of FM-MOF-6

The activated FM-MOF-7 (0.100 g) and azobisisobutyronitrile (AIBN, 0.010 g) were added to 1,2-Ethanedithiol (4 ml). The mixture was stirred and heated to 80 °C for 48 h under N_2 atmosphere. The resultant precipitate was obtained by centrifugation, washed with acetone several times, and then dried overnight under vacuum condition to produce the solid of FM-MOF-6.

Synthesis of FM-MOF-9

The activated MOF-808 (0.100 g) was added to bromoacetic acid (0.700 g) in a solution containing 10 ml of DMF. The mixture was stirred and heated to 60°C for 24 h under N_2 atmosphere. The resultant precipitate was obtained by centrifugation, washed with DMF and acetone several times, and then dried at 60 °C overnight under vacuum condition to produce the solid of FM-MOF-9.

Synthesis of FM-MOF-8

The activated FM-MOF-9 (0.200 g) was added to 1-allylimidazole (2 ml) in a solution containing 18 ml of acetonitrile. The mixture was stirred and heated to 80°C for 12 h under N_2 atmosphere, and then continued to react for another 12 h when the system was cooled to room temperature. The resultant precipitate was obtained by

centrifugation, washed with DMF and acetone several times, and then dried at 60 °C overnight under vacuum condition to produce the solid of FM-MOF-8.

Synthesis of FM-MOF-1-4

The activated FM-MOF-1 (0.100 g) was added to 1-pyrenecarboxylic acid (0.800 g) in a solution containing 10 ml of DMF. The mixture was stirred and heated to 60°C for 24 h under N_2 atmosphere. The resultant precipitate was obtained by centrifugation, washed with DMF and acetone several times, and then dried under vacuum condition to produce the solid of FM-MOF-1-4.

Adsorption experiments

Metal ions adsorption isotherms. To obtain metal ions adsorption isotherms, FM-MOF sample (0.010 mg) was added into 10 ml aqueous solutions with different concentrations of metal ions. The mixture was shaken in an incubated shaker at room temperature for 48 h to ensure that adsorption equilibrium had been reached. The treated solutions were filtered through a 0.22 μm membrane filter. Subsequently, the filtrates were measured by using ICP to determine the remaining metal ions concentration. The adsorption capacity at equilibrium, q_e (mg g^{-1}), was calculated as follows:

$$q_e = \frac{(c_0 - c_e) \times V}{m}$$

where c_0 and c_e are the initial and final equilibrium concentrations of metal ions (mg L^{-1}) in the solution, respectively. V is the volume of the testing solution (ml), and m represents the amount of adsorbent (g). In order to estimate the metal ions uptake capacities of FM-MOFs, the experimental data were fitted with the Langmuir isotherm model using the following equation[24]:

$$\frac{c_e}{q_e} = \frac{1}{q_m k_L} + \frac{c_e}{q_m}$$

where q_e (mg g^{-1}) and c_e (mg L^{-1}) are the adsorbed amount of metal ions on the adsorbent and the metal ions concentration at equilibrium, q_m (mg g^{-1}) is the saturated sorption capacity at monolayer, and k_L is the Langmuir constant.

Metal ions adsorption kinetics. FM-MOF sample (0.010 g) was added into 10 ml aqueous solution of metal ions with a concentration of 10 ppm. The mixture was shaken in an incubated shaker at room temperature for 24 h. During the adsorption period, the mixture was filtered at appropriate time intervals through a 0.22 μm membrane filter. Subsequently, the filtrates were measured by using ICP to determine the residual metal ions concentration. These experimental data were fitted with the pseudo-second-order kinetic model using the following equation[25].

$$\frac{t}{q_t} = \frac{1}{k_2 q_e^{\,2}} + \frac{t}{q_e}$$

where q_t (mg g^{-1}) and q_e (mg g^{-1}) are sorption quantity of metal ions at time t (min) and at equilibrium, and k_2 (g $mg^{-1}min^{-1}$) is the rate constant of the pseudo-second-order equation.

Fluorescence experiments

In a typical experimental setup, 2 mg of FM-MOF sample was added into 2 ml of prepared analyte solutions with different concentrations. The mixture was shaken in an incubated shaker at room temperature for 24 h. Subsequently, the mixture was sonicated for a few minutes to maintain the homogeneity of the solution before luminescent measurements. For all measurements, the dispersed solutions of FM-MOFs were excited at λ_{ex} = 279 nm.

Catalytic experiments

In a typical catalytic cycloaddition, 10 mmol epoxides and catalyst (0.09 g, 0.5 mol%) were placed in a Schlenk tube. The reaction mixture was stirred at 80 °C for 12 h and 0.1 MPa CO_2 atmosphere. The yields were calculated according to ^{1}H NMR analysis.

Proton conductivity measurements.

The MOF powder (ca. 50 mg) was pressed at 1000 kg cm^{-2} pressure for 2 min to make a pellet (6 mm in diameter). Both sides of the pellet were attached to silver wires with silver paste and then sealed in a homemade double-walled glass chamber. The relative humidity (RH) inside the chamber was controlled by different saturated salt aqueous solutions as reported previously[26,27]. The impedance was measured at

room temperature by using a CHI660E electrochemical workstation. The proton conductivity (σ, S cm^{-1}) of the sample was estimated as follows:

$$\delta = \frac{L}{RA}$$

where L (cm) is the thickness of the pellet, R (Ω) is the impedance, and A (cm^2) is the face area of the pellet.

Modules switching process

Transformation from FM-MOF-2 to FM-MOF-9. The activated FM-MOF-2 (0.100 g) was added to bromoacetic acid (0.700 g) in a solution containing 10 ml of DMF. The mixture was stirred and heated to 60°C for 24 h under N_2 atmosphere. This process can be repeated several times to ensure full conversion.

Transformation from FM-MOF-2 to FM-MOF-7. The activated FM-MOF-2 (0.100 g) was added to propenoic acid (2 ml) in a solution containing 10 ml of acetonitrile. The mixture was stirred and heated to 60°C for 24 h under N_2 atmosphere. This process can be repeated several times to ensure full conversion.

Transformation from FM-MOF-9 to FM-MOF-2. The activated FM-MOF-9 (0.100 g) was added to propiolic acid (2 ml) in a solution containing 10 ml of acetonitrile. The mixture was stirred and heated to 60°C for 24 h under N_2 atmosphere. This process can be repeated several times to ensure full conversion.

Transformation from FM-MOF-9 to FM-MOF-7. The activated FM-MOF-9 (0.100 g) was added to propenoic acid (2 ml) in a solution containing 10 ml of acetonitrile. The mixture was stirred and heated to 60°C for 24 h under N_2 atmosphere. This process can be repeated several times to ensure full conversion.

Transformation from FM-MOF-7 to FM-MOF-2. The activated FM-MOF-7 (0.100 g) was added to propiolic acid (2 ml) in a solution containing 10 ml of acetonitrile. The mixture was stirred and heated to 60°C for 24 h under N_2 atmosphere. This process can be repeated several times to ensure full conversion.

Transformation from FM-MOF-7 to FM-MOF-9. The activated FM-MOF-7 (0.100 g) was added to bromoacetic acid (0.700 g) in a solution containing 10 ml of DMF. The mixture was stirred and heated to 60°C for 24 h under N_2 atmosphere. This process can be repeated several times to ensure full conversion.

REFERENCES

1. Hou H, Yu D, Hu G. Preparation and properties of ion-imprinted hollow particles for the selective adsorption of silver ions. *Langmuir* 2015;31:1376-84.[PMID:25587633 DOI:10.1021/la5032784]

2. Yao Y, Gao B, Wu F, Zhang C, Yang L. Engineered biochar from biofuel residue: characterization and its silver removal potential. *ACS Appl Mater Interfaces* 2015;7:10634-40.[PMID:25923987 DOI:10.1021/acsami.5b03131]

3. Zhang M, Zhang Y, Helleur R. Selective adsorption of Ag^+ by ion-imprinted O-carboxymethyl chitosan beads grafted with thiourea-glutaraldehyde. *Chemical Engineering Journal* 2015;264:56-65.[DOI:10.1016/j.cej.2014.11.062]

4. Wang L, Wang K, Huang R, Qin Z, Su Y, Tong S. Hierarchically flower-like WS_2 microcrystals for capture and recovery of Au (III), Ag (I) and Pd (II). *Chemosphere* 2020;252:126578.[PMID:32443268 DOI:10.1016/j.chemosphere.2020.126578]

5. Pan X, Fu L, Wang H, Xue Y, Zu J. Synthesis of novel sulfydryl-functionalized chelating adsorbent and its application for selective adsorption of Ag(I) under high acid. *Separation and Purification Technology* 2021;271:118778.[DOI:10.1016/j.seppur.2021.118778]

6. Hassanzadeh Fard Z, Malliakas CD, Mertz JL, Kanatzidis MG. Direct extraction of Ag^+ and Hg^{2+} from cyanide complexes and mode of binding by the layered $K_2MgSn_2S_6$ (KMS-2). *Chem Mater* 2015;27:1925-8.[DOI:10.1021/acs.chemmater.5b00374]

7. Ma L, Wang Q, Islam SM, Liu Y, Ma S, Kanatzidis MG. Highly selective and efficient removal of heavy metals by layered double hydroxide intercalated with the MoS4(2-) ion. *J Am Chem Soc* 2016;138:2858-66.[PMID:26829617 DOI:10.1021/jacs.6b00110]

8. Zhou Y, Gao B, Zimmerman AR, Cao X. Biochar-supported zerovalent iron reclaims silver from aqueous solution to form antimicrobial nanocomposite. *Chemosphere* 2014;117:801-5.[PMID:25461951 DOI:10.1016/j.chemosphere.2014.10.057]

9. Asiabi H, Yamini Y, Shamsayei M, Molaei K, Shamsipur M. Functionalized layered double hydroxide with nitrogen and sulfur co-decorated carbondots for highly selective and efficient removal of soft Hg^{2+} and Ag^{+} ions. *J Hazard Mater* 2018;357:217-25.[PMID:29890418 DOI:10.1016/j.jhazmat.2018.05.055]
10. Das R, Giri S, King Abia AL, Dhonge B, Maity A. Removal of Noble Metal Ions (Ag^{+}) by mercapto group-containing polypyrrole matrix and reusability of its waste material in environmental applications. *ACS Sustainable Chem Eng* 2017;5:2711-24.[DOI:10.1021/acssuschemeng.6b03008]
11. Yee KK, Reimer N, Liu J, et al. Effective mercury sorption by thiol-laced metal-organic frameworks: in strong acid and the vapor phase. *J Am Chem Soc* 2013;135:7795-8.[PMID:23646999 DOI:10.1021/ja400212k]
12. Hou YL, Yee KK, Wong YL, et al. Metalation triggers single crystalline order in a porous solid. *J Am Chem Soc* 2016;138:14852-5.[PMID:27794594 DOI:10.1021/jacs.6b09763]
13. Luo F, Chen JL, Dang LL, et al. High-performance Hg^{2+} removal from ultra-low-concentration aqueous solution using both acylamide- and hydroxyl-functionalized metal-organic framework. *J Mater Chem A* 2015;3:9616-20.[DOI:10.1039/c5ta01669j]
14. Zhao M, Huang Z, Wang S, Zhang L, Zhou Y. Design of l-cysteine functionalized UiO-66 MOFs for selective adsorption of Hg(II) in aqueous medium. *ACS Appl Mater Interfaces* 2019;11:46973-83.[PMID:31746183 DOI:10.1021/acsami.9b17508]
15. Shi M, Lin D, Huang R, Qi W, Su R, He Z. Construction of a mercapto-functionalized Zr-MOF/melamine sponge composite for the efficient removal of oils and heavy metal ions from water. *Ind Eng Chem Res* 2020;59:13220-7.[DOI:10.1021/acs.iecr.0c00731.s001]
16. Liang L, Chen Q, Jiang F, et al. In situ large-scale construction of sulfur-functionalized metal-organic framework and its efficient removal of Hg(ii) from water. *J Mater Chem A* 2016;4:15370-4.[DOI:10.1039/c6ta04927c]
17. Liang L, Liu L, Jiang F, et al. Incorporation of In_2S_3 nanoparticles into a metal-organic framework for ultrafast removal of hg from water. *Inorg Chem* 2018;57:4891-7.[PMID:29693386 DOI:10.1021/acs.inorgchem.7b03076]
18. Jiang SY, He WW, Li SL, Su ZM, Lan YQ. Introduction of molecular building blocks to improve the stability of metal-organic frameworks for efficient mercury

removal. *Inorg Chem* 2018;57:6118-23.[PMID:29737154 DOI:10.1021/acs.inorgchem.8b00704]
19. Li J, Duan Q, Wu Z, et al. Few-layered metal-organic framework nanosheets as a highly selective and efficient scavenger for heavy metal pollution treatment. *Chemical Engineering Journal* 2020;383:123189.[DOI:10.1016/j.cej.2019.123189]
20. Mon M, Lloret F, Ferrando-soria J, Martí-gastaldo C, Armentano D, Pardo E. Selective and efficient removal of mercury from aqueous media with the highly flexible arms of a BioMOF. *Angew Chem* 2016;128:11333-8.[PMID:27529544 DOI:10.1002/anie.201606015]
21. Fu K, Liu X, Lv C, et al. Superselective Hg(II) removal from water using a thiol-laced MOF-based sponge monolith: performance and mechanism. *Environ Sci Technol* 2022;56:2677-88.[PMID:35112842 DOI:10.1021/acs.est.1c07480]
22. Furukawa H, Gándara F, Zhang YB, et al. Water adsorption in porous metal-organic frameworks and related materials. *J Am Chem Soc* 2014;136:4369-81.[PMID:24588307 DOI:10.1021/ja500330a]
23. Jiang J, Gándara F, Zhang YB, Na K, Yaghi OM, Klemperer WG. Superacidity in sulfated metal-organic framework-808. *J Am Chem Soc* 2014;136:12844-7.[PMID:25157587 DOI:10.1021/ja507119n]
24. Langmuir I. The adsorption of gases on plane surfaces of glass, mica and platinum. *J Am Chem Soc* 1918;40:1361-403.[DOI:10.1021/ja02242a004]
25. Li F, Wang X, Yuan T, Sun R. A lignosulfonate-modified graphene hydrogel with ultrahigh adsorption capacity for Pb(ii) removal. *J Mater Chem A* 2016;4:11888-96.[DOI:10.1039/c6ta03779h]
26. Taylor JM, Mah RK, Moudrakovski IL, Ratcliffe CI, Vaidhyanathan R, Shimizu GK. Facile proton conduction via ordered water molecules in a phosphonate metal-organic framework. *J Am Chem Soc* 2010;132:14055-7.[PMID:20857972 DOI:10.1021/ja107035w]
27. Liang X, Zhang F, Feng W, et al. From metal-organic framework (MOF) to MOF-polymer composite membrane: enhancement of low-humidity proton conductivity. *Chem Sci* 2013;4:983-92.[DOI:10.1039/c2sc21927a]